Isern, A.R., Anselmetti, F.S, Blum, P., et al., 2002
Proceedings of the Ocean Drilling Program, Initial Reports Volume 194

2. Explanatory Notes[1]

Shipboard Scientific Party[2]

INTRODUCTION

Information assembled in this chapter will help the reader understand the basis for the preliminary conclusions and also enable the interested investigator to select samples for further analysis. This information concerns only shipboard operations and analyses described in the site reports in the Leg 194 *Initial Reports* of the *Proceedings of the Ocean Drilling Program*. Methods used by various investigators for shore-based analyses of Leg 194 data will be described in the individual contributions published in the *Scientific Results* volume and in publications within various professional journals.

Drilling Operations

Three standard coring systems were used during Leg 194: the advanced piston corer (APC), the extended core barrel (XCB), and the rotary core barrel (RCB). These standard coring systems and their characteristics are summarized in the "Explanatory Notes" chapters of previous *Initial Reports* volumes as well a number of technical notes. The Leg 139 *Initial Reports* volume includes a particularly detailed description. In addition, the developmental advanced diamond coring barrel (ADCB) system was deployed for the second time (first time during Leg 193) and is described in some detail below. All systems were applied to maximize core recovery in the sediments being cored. Most cored intervals were ~9.6 m long, which is the length of a standard core barrel. In some cases, the RCB was advanced only part of the interval to maximize recovery. ADCB core barrels were 4.8 m long. In some holes the drill string was drilled, or "washed ahead," without recovering sediments in order to advance the drill bit to a target depth where core recovery needed to be resumed.

[1]Examples of how to reference the whole or part of this volume.
[2]Shipboard Scientific Party addresses.

Ms 194IR-102

Drilled intervals are measured from the kelly bushing on the rig floor to the bottom of the drill pipe and referred to in meters below rig floor (mbrf). Meters below seafloor (mbsf) references for the core tops are calculated by subtracting the seafloor depth. When sediments of substantial thickness cover the seafloor (as at all but one site during Leg 194), the mbrf depth of the seafloor is determined with a mudline core, assuming 100% recovery for the cored interval in the first partly filled core barrel. Water depth is calculated by subtracting the distance from the rig floor to sea level from the mudline measurement in mbrf. This water depth usually differs from precision depth recorder measurements by a few to several meters.

Sea Trials with the Advanced Diamond Core Barrel

The diamond core barrel (DCB) was developed in 1990 as a spin-off project of the diamond coring system's drill-in bottom-hole assembly seafloor hardware project. The DCB provided an alternative method to the RCB system for obtaining hard rock cores. The DCB used the same inner barrel as the RCB but was packaged inside 6-in drill collars in place of the larger 8-in drill collars used for the rest of the Ocean Drilling Program (ODP) coring systems. Even though the 6-in drill collar connection is slightly underbalanced, it does not present any strength problems as long as it is not used for bare-rock spudding. It can be operated inside an existing hole or casing.

The ADCB takes the DCB one step further by using a different inner barrel while maintaining the same size 6-in outer barrel. These dimensions allow the bit to have a thinner kerf width (1.95 in), similar to mining-style core barrels (typically 0.96 in), compared to that of the RCB (3.78 in) (Table T1). The ADCB must be considered a hybrid, thick kerf system even though it more closely approximates a conventional mining-style DCB.

T1. Comparison of core barrels, p. 51.

The rational for the smaller inner barrel diameter is not necessarily a larger core diameter, but increased bit life. Thick kerf diamond bits have shown excessive wear because the inner portion of the bit cuts at a significantly slower rate than the outer portion of the bit (known as "ringing"). Mining systems can operate with a much thinner kerf than the ADCB because they can operate with drill rods, which do not have the upset tool joints. These types of thin rods must be laterally supported; otherwise the connections will fail. In an offshore environment, this type of rod can only be used within a riser pipe. ODP open hole operations must use strong enough connections to allow for vessel offsets due to currents and surface sea states. Based on the combination of connection strength and economic and operational constraints aboard the *JOIDES Resolution,* a hole diameter was set at 7 in, maintaining a packed hole condition with 6-in drill collars.

Earlier attempts at using diamond bits resulted in only marginal success. This was primarily due to the inability of the passive heave compensator to keep the bit on the bottom of the hole. Diamond bits generally require less weight than roller cone bits, and the breakaway seal friction in the *JR*'s passive cylinders alone was sometimes more than the weight-on-bit requirements, particularly in a shallow borehole. Therefore, the timing of the ADCB project was intended to dovetail the installation of the new active heave compensator (AHC), which should eliminate much of the weight fluctuation on the bit. By the time of Legs 193 and 194, installation of the AHC and training of personnel had been completed. Unfortunately, the AHC acted erratically at mod-

erate to high sea states, when it was needed most, and had to be turned off during some of the ADCB drilling on Leg 194.

A proven and robust inner core barrel was selected "off the shelf" (Boart Longyear's PQ inner barrel hardware). This was primarily done to keep the project expenses within the allocated budget and to avoid reinventing or redesigning hardware until it was determined that enhancements were indeed needed. A few modifications were made including a new positive indicator latch.

The core obtained from the new ADCB inner barrel produces over twice the core volume per unit length compared with the RCB. The ADCB core is available in two sizes (Table T1). The double tube core barrel (outer barrel and inner barrel; referred to as PQ barrel) is run without a liner and cuts a 3.345-in cores. The triple tube system (PQ3 barrel) is run with or without metal split liners (wall thickness of 0.065 in or 1.65 mm) or lexan liners (wall thickness of 0.05 in) and cuts a 3.27-in core. The PQ3 barrel with lexan liners was used during Leg 194.

The ADCB offers the following advantages over the RCB in certain applications:

1. Improved core quality,
2. Better hole stability,
3. Increased core recovery,
4. Less hole disturbance,
5. Smaller hole diameter,
6. Less susceptibility to becoming stuck,
7. Easier hole cleaning because of smaller cuttings, and
8. Potentially better logging results.

The ADCB also can be configured in either a 15 ft (4.75 m) or a 30 ft (9.5 m) version. The shorter version, used during Leg 194, is the preferred version in which to operate the ADCB.

The ADCB will require pulling short cores more often than with the RCB. Once a core jams it is unlikely that further advancement of the outer barrel will occur, and continued advancement will lead to faster bit destruction and loss of time for round trips to change bits. While interval drilling may be possible in soft, friable formations such as the reefal limestone drilled on Leg 194, it is doubtful that it can be performed in hard crystalline rock where the more sensitive ADCB inner barrel components, as well as the bit, might be damaged.

Operating flow rates for the ADCB are 35 to 150 gal/min, which is significantly less than the rates used for roller cone bits. Cuttings produced by a diamond bit are much smaller and the amount per length of core is less than half that of the RCB. With the ADCB, a drop in pressure will notify the driller immediately of a core block, and a threshold pressure that must first be overcome will notify the driller that the core barrel has landed and successfully latched in place. This is accomplished by forcing all the flow through a regulated valve within the latch once the core barrel has landed.

Curatorial Procedures and Sample Depth Calculations

Numbering of sites, holes, cores, and samples follows the standard ODP procedure. A full curatorial identifier for a sample consists of the leg, site, hole, core number, core type, section number, and interval in centimeters measured from the top of the core section. For example, a sample identification of 194-1192A-1H-1, 10–12 cm, would represent a

sample removed from the interval between 10 and 12 cm below the top of Section 1, Core 1 of Hole 1192A during Leg 194 (H designates that this core was taken with the APC system; R stands for RCB, X for XCB, and Z for ADCB cores). Cored intervals are also referred to in "curatorial" mbsf. The mbsf depth of a sample is calculated by adding the depth of the sample below the section top and the lengths of all higher sections in the core to the core-top datum measured with the drill string.

A sediment core from less than a few hundred mbsf may, in some cases, expand upon recovery (typically 10% in the upper 300 m), in which case its length will not match the drilled interval. In addition, a coring gap typically occurs between cores, as shown by composite depth construction (see the *Initial Reports* volumes for Legs 138, 177, and 184 [Shipboard Scientific Party 1992, 1999a, 2000]). Thus, a discrepancy may exist between the drilling mbsf and the curatorial mbsf. For instance, the curatorial depth (mbsf) of a sample taken from the bottom of a core may be larger than that of a sample from the top of the subsequent core. During Leg 194, multiple APC/XCB holes were not cored and continuous composite sections, therefore, could not be constructed.

If a core has incomplete recovery, all cored material is assumed to originate from the top of the drilled interval as a continuous section for curation purposes. The true depth interval within the cored interval is not known, resulting in an uncertainty, for instance, in age-depth analysis and correlation of core facies with downhole log signals.

Core Handling and Analysis

General core handling procedures are described in previous *Initial Reports* volumes and the *Shipboard Scientist's Handbook* and are only summarized here. As soon as cores arrived on deck, gas void and headspace samples were taken by means of a syringe (if applicable) for immediate analysis as part of the shipboard safety and pollution prevention program. Core catcher samples were obtained for biostratigraphic analysis. When the core was cut in sections, whole-round samples were taken for shipboard interstitial water analysis. In addition, headspace-gas samples were immediately extracted from the ends of cut sections and sealed in glass vials for light-hydrocarbon analysis.

Before splitting, whole-round core sections were run through the multisensor track (MST), and thermal conductivity measurements were taken. Additional whole-round samples were taken at that point for postcruise research. The cores were then split into working and archive halves (from bottom to top), so investigators should be aware that older material could have been transported upward on the split face of each section. When short pieces of sedimentary rock were recovered, the individual pieces were split with the rock saw and placed in split liner compartments created by sealing spacers into the liners with acetone.

Curation methods had to be improvised for the larger diameter ADCB cores. The lexan liners used to retrieve the cores imposed two problems: (1) when split, the edges warped inside, and (2) the plastic spacers could not be sealed onto that material with acetone. No long intact core sections were recovered with the ADCB, so the procedure was limited to rock pieces of maximum 30-cm length. The core pieces were moved into a "liner patch," which is a liner with a diameter between those of the regular core liner and the ADCB lexan liner. Liner patch is usually used to bandage broken regular liners. It was divided into compartments of appropriate size using slightly modified plastic spacers

and placed in a D-shaped cross section tube that had the top cut off, which provided the additional strength needed. The top of the core section was always measured from the top of the blue end cap glued into the liner patch and not from the top of the D-tube. ADCB core pieces were then placed in the new customized liner and, after sampling was completed, shrink-wrapped for safe transport.

Coherent and reasonably long archive-half sections were measured for color reflectance using the archive-half multisensor track. All archive-half sections were run through the cryogenic magnetometer, described visually and by means of smear slides and thin sections, and photographed with both black-and-white and color film. Close-up photographs were taken of particular features for illustrations in site summaries as requested by individual scientists. During Leg 194, a digital close-up imaging system was installed for the first time and used extensively. All images are available from the ODP database (TIF or JPEG format; ~0.5- to ~20-MB file sizes). Compressed JPEG versions (~0.5 MB) were written to CD-ROM on the ship and distributed to shipboard scientists.

The working half was sampled both for shipboard analysis including physical properties, further sedimentologic and biostratigraphic analyses, carbonate, and bulk X-ray diffraction (XRD) mineralogy, and for shore-based studies. Both halves of the core were then put into labeled plastic D-tubes, sealed, and placed in cold storage space aboard the ship. At the end of the leg, the cores were transferred from the ship into refrigerated containers and shipped to the ODP Gulf Coast Core Repository in College Station, Texas.

LITHOSTRATIGRAPHY AND SEDIMENTOLOGY

Sediment and Rock Classification

Analysis of rocks and sediments starts with the recognition, identification, and physical description of individual sedimentary grains. Based on the suite of grain types and texture that results, sediments and rocks can be classified. Hence, this section consists of two parts: (1) grain type and (2) sediment and rock classification.

Grain Types

Grain types in granular sediments and rocks were classified in five categories according to mineralogy and origin:

1. Pelagic calcareous and siliceous. Pelagic sediments are characterized by fine-grained skeletal debris primarily produced within the upper part of the water column in an open-marine environment by calcareous microfauna and microflora (e.g., foraminifers, pteropods, and nannofossils) and siliceous microfauna and microflora (e.g., diatoms and radiolarians). During Leg 194, only very minor amounts of siliceous microfossils were recognized.
2. Hemipelagic calcareous and siliceous. Hemipelagic sediments contain the same components as pelagic sediments with the addition of >10% neritic carbonate and/or siliciclastic material. Because of the continental margin setting of the Marion Plateau and the influence of carbonate platform sedimentation, virtually all nonneritic sediments were deemed to be hemipelagic.

3. Neritic calcareous and siliceous. Neritic sediments consist of coarse- to fine-grained particles originating from shallow-water areas (e.g., platform upper slope or periplatform) and consist mostly of carbonate skeletal (i.e., bioclastic) components, nonskeletal fragments, and micrite. The term micrite is used to define very fine calcareous particles (<20 µm) of various origin. Neritic carbonate grains (Tucker and Wright, 1990) observed during Leg 194 include the following:

    a. Skeletal components. These include the remains of large and small benthic foraminifers, bivalves, gastropods, coralline algae, corals, bryozoans, echinoderms, and minor green algae. Additionally, rhodoliths were commonly observed. These consisted of gravel-sized (≤60 mm in diameter), subspherical nodules of concentrically encrusted coralline algae.
    b. Nonskeletal components. Minor intraclasts and lithoclasts were occasionally encountered. Ooids, peloids, pellets, and oncolites were problematic; they may be present in some lithologies, but extensive dolomitization prevented positive identification.

4. Siliciclastic. Siliciclastic grains, composed of quartz, feldspar, mica, and rock fragments that were eroded from igneous, metamorphic, and noncarbonate sedimentary rocks were observed in some intervals.
5. Marine noncarbonate authigenic minerals. Phosphate and glauconite were the most common authigenic minerals observed. Glauconite is a black to greenish, iron-rich sheet silicate, which can infill test chambers and pores or appear as rounded sand-sized grains. Phosphates constitute a complex family of phosphorous-rich minerals. They are commonly black and occur as sand-sized grains. Unoxidized framboidal pyrite was also commonly found.

Principal Rock Names

Principal names of the sediments and rocks observed are formulated on the basis of composition and texture in conjunction with major and minor modifiers. Four main categories of principal rock names were used: (1) carbonates (including dolomitized limestones and dolostones); (2) siliciclastics; (3) mixed carbonate and siliciclastics, which are further subdivided as carbonate-dominant and siliciclastic-dominant; and (4) basement (Fig. F1).

Major and Minor Modifiers

To describe the lithology of the granular sediments and rocks in greater detail, the principal name (i.e., grainstone) is often preceded by a major modifier (i.e., skeletal) and followed by minor modifiers. Minor modifiers are preceded by the term "with" (for example, "skeletal grainstone with clay"). Minor modifiers associated with principal names were used sparingly for simplicity. Minor modifiers were used to supply greater detail in the "Lithologic Description" section of the barrel sheets (see the "Core Descriptions" contents list). In general, the most common use of major and minor modifiers was to describe grain types that were present in major (>25%) and minor (<25%) proportions. In addi-

F1. Graphic symbols for three main sediment and rock categories and basement, p. 40.

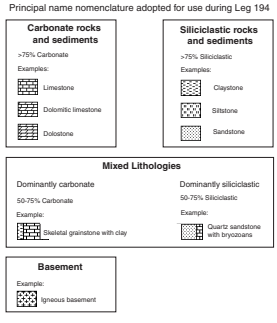

tion, major modifiers were used to provide additional information on grain size, constituent mineralogy, and rock composition.

Carbonate Nomenclature

For pure carbonate lithologies (0%–25% noncarbonate grains), the original Dunham (1962) textural classification was applied in conjunction with the depositional textures described by Embry and Klovan (1971) (Fig. F2). Following Dunham (1962), carbonate crystals or fragments that are smaller than 20 µm (hence not visible with a hand lens) are referred to as micrite. Constituents >20 µm are called grains. For clarity, we used the definitions cited below:

1. Mudstone = mud-supported fabric with <10% grains.
2. Wackestone = mud-supported fabric with >10% grains.
3. Packstone = grain-supported fabric with intergranular mud.
4. Grainstone = grain-supported fabric with no mud.
5. Floatstone = matrix-supported fabric (at least 10% of grains >2 mm in size).
6. Rudstone = grain-supported fabric (at least 10% of grains >2 mm in size).
7. Boundstone = components organically bound during deposition.

Matrix in floatstones and rudstones may be anything from mudstone to grainstone. For example, a sediment with 10-mm-diameter rhodoliths in grain contact with each other and having a skeletal grainstone matrix is a rudstone.

Subdivisions within this group include

a. Bafflestone: formed by organisms that act as baffles;
b. Bindstone: formed by organisms that encrust or bind; and
c. Framestone: formed by organisms that build a rigid framework.

In lithologies where the dominant grain size was 20–63 µm and the sediments were well-sorted with grains in contact with each other, we placed the major modifier "silt-sized" before Dunham's (1962) principal name (e.g. silt-sized grainstone). The major modifier "skeletal" was not used in this case if the bioclastic components could not be identified because of the fine grain size. Modifiers such as "fine sand-sized" are also used to refine the description of sand-sized grainstones in the "Lithologic Description" section on the barrel sheets.

The major modifiers "skeletal" and "nonskeletal" are used to indicate the occurrence of bioclastic fragments and nonbioclastic allochems (e.g., ooids), respectively, within the carbonate sediments. The lack of such a modifier implies that components have not been identified or that the sediments include an even proportion of skeletal and nonskeletal allochems. If the nonskeletal components exceed 25%, then the lithology is determined to be nonskeletal.

Whenever dolomite or dolomitic texture was recognized (>25%) in carbonate sediments, the term "dolomitic" was used as a major modifier (e.g., dolomitic mudstone with clay). When a lithology appeared to contain >~75% dolomite, it was called "dolostone" or, if skeletal components can be recognized, "skeletal dolostone."

F2. Dunham (1962) classification of limestones, p. 41.

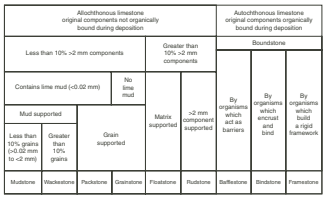

Siliciclastic Sediments and Rocks

The nomenclature of siliciclastic sediments and rocks (>50% clay = claystone; >50% silt = siltstone; and >50% sand = sandstone) is based on the Udden-Wentworth grain size scale (Fig. F3) (Wentworth, 1922). Grain mineralogy is expressed by both major and minor modifiers (i.e., quartz sandstone with glauconite). Modifiers for mixed grain sizes (i.e., silty claystone) are used in accordance with Figure F4 (Shepard, 1954). When two or more textural groups or subgroups are present, the principal names appear in order of increasing abundance.

Mixed Carbonate and Siliciclastic Rocks and Sediments

Carbonate-dominated sediments and rocks (50%–75% carbonate) were described as pure carbonates with the grain size of the siliciclastic fraction added as a major modifier after the principal name (e.g., skeletal wackestone with quartz) (Fig. F1). Siliciclastic-dominated lithologies (>50%–75% siliciclastic) were described as pure siliciclastic rocks and sediments with the addition of the main carbonate constituent after the principal name (e.g., quartz siltstone with bryozoans) (Fig. F1).

Basement Rocks

Basement rocks that were recovered are lithologically complex and difficult to characterize in hand specimens, and thin section petrography was used to better characterize these horizons. All basement rocks encountered were either olivine basalt or breccia deriving from those basalts (Fig. F1).

Sediment Core Description

General Procedure

Leg 194 sedimentologists adopted the following strategy before writing comments on the visual core description (VCD) form used for each core section (Fig. F5):

1. The core was examined to pick boundaries, determine lithologies, identify key features, and determine the samples to be collected (i.e., smear slide, thin section, and/or close-up photograph sites).
2. Cores were then described in detail on VCDs following the procedure outlined in the next section. The archive halves of soft-sediment cores (not segmented rock fragments) were analyzed with the MST to obtain color reflectance data (see "Core Physical Properties," p. 21). Other than for the upper part of Site 1192, magnetic susceptibility data were not collected with the MST. Additionally, digital photographs were taken on a separate track installed for the first time during Leg 194 (see below).
3. Information recorded on the VCDs were then entered on a computer using the AppleCORE program (version 8.1) to produce the barrel sheets (see the "Core Descriptions" contents list).
4. Ultimately, data from the barrel sheets coming from different holes at a site were compiled into one figure and one table used to distinguish lithologic units. These figures can be found in the "Lithostratigraphy and Sedimentology" section of each site chapter in this volume.

F3. Udden-Wentworth grain-size classification, p. 42.

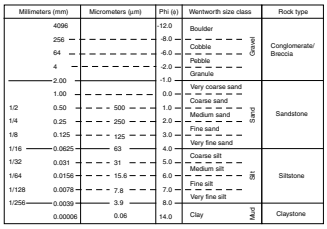

F4. Classification scheme used for siliciclastic sediments, p. 43.

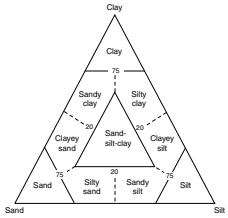

F5. Visual core description sheet, p. 44.

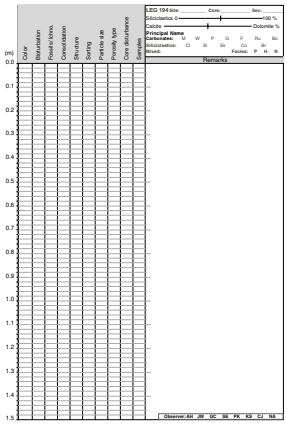

Visual Core Descriptions

The VCD form used on previous ODP legs was modified to meet the specifics of sediments and rocks encountered during Leg 194 and to facilitate data entry into the AppleCORE program (Fig. F5). Description guidelines were established to homogenize the observations made by different shifts and by scientists within a shift (Table T2).

T2. Checklist for visual core description forms, p. 52.

Barrel Sheets

The sediment core description forms, or barrel sheets, summarize shipboard observations and descriptions of the sediments retrieved in each core (Fig. F6). A barrel sheet uses the separate VCDs established for each section (including the core catcher). Effectively presenting information on the barrel sheets often required a nonquantitative, subjective reduction and synthesis of data from the VCDs. Leg 194 scientists supplemented the available symbols in the AppleCORE program in order to graphically display the sediments encountered (Fig. F7).

The ODP conventions used for the compilation of barrel sheets and the modifications to these procedures adopted by the Leg 194 Shipboard Scientific Party are described below. The order of the following headers reflects the order from left to right of the columns in the barrel sheets (see Fig. F6):

1. Meters: This column lists the nominal depth below seafloor (mbsf) of the core.
2. Core and section: Each core was cut into 1.5-m sections and numbered according to ODP convention. The core and section number are listed in this column.
3. Texture: Textural classifications are represented here by a vertical line displayed in the appropriate column (Fig. F6). For siliciclastics or dolostone where texture was lost, this column was left blank.
4. Graphic lithology: Lithologies were represented by patterns (Fig. F1) displayed in the graphic lithology column. Mixed lithologies were indicated on the barrel sheets by splitting the graphic symbol vertically, with the width of each pattern showing the relative proportions of constituents.
5. Bioturbation: Five degrees of bioturbation were differentiated (Fig. F7), similar to the scheme of Droser and Bottjer (1986), and are shown in the "Bioturbation" column on the barrel sheet (Fig. F6). Bioturbation ranges in degree from "barren" to "abundant," with "rare," "moderate," and "common" in between.
6. Structures, accessories, ichnofossils, fossils: These four categories are represented in the same column. The location and nature of primary sedimentary structures (e.g., planar laminations) and deformational structures (e.g., microfaults) are shown in the "Structure" column of the barrel sheet (Fig. F6). Lithologic accessories include a variety of structures, nonskeletal grains, and diagenetic features such as pyrite concretions. Finally, occurrences of ichnofossils and major groups of macro- and microfossils were also graphically indicated in this column.
7. Core disturbance: Observations of drilling-related disturbance over an interval of 20 cm or more were recorded in the "Disturbance" column using the symbols shown in Figure F7. The degree of drilling disturbance in *soft and firm sediments* is as follows:

F6. Completed core description form, p. 45.

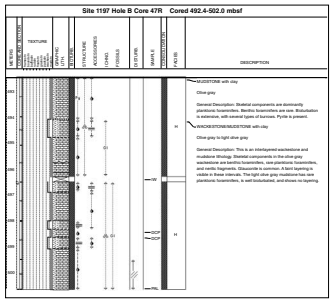

F7. Graphic symbols used in barrel sheets, p. 46.

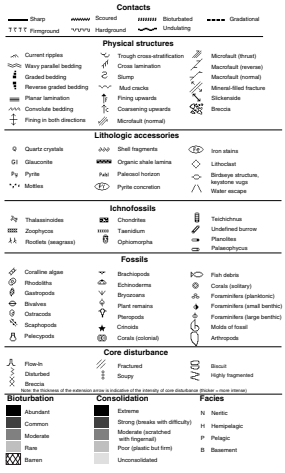

a. Slightly disturbed: Bedding contacts are slightly deformed.
b. Moderately disturbed: Bedding contacts have undergone extreme bowing.
c. Very disturbed: Bedding is completely deformed by flowing coring/drilling slough and other soft sediment, or by stretching and/or compressional shearing structures attributed to the boring/drilling.
d. Soupy: Intervals are water saturated and have lost all aspects of original bedding.

The degree of disturbance in *indurated* sediments and rocks is described using the following categories:

a. Fractured (in various degrees of severity): Core pieces are in place and broken or partly displaced from their original orientation.
b. Biscuits (in various degrees of severity): Uniquely shaped, rounded, oblong rock fragments preserved or recognizable (drilling slurry may surround these fragments).
c. Fragmented (in various stages of severity): Core pieces are probably in correct stratigraphic sequence although they may not represent the entire sequence. The original orientation is lost. The fragments were each separately stored and archived within small plastic partitions within each half-core tube.
d. Drilling breccia: The rocks are crushed and broken into many small and angular or rounded pieces with the original orientation and stratigraphic position lost. Often drilling breccia is completely mixed with drilling slurry.

8. Samples: Samples taken from each core for analysis are indicated in the "Sample" column of the barrel sheets. SS = smear slide, THS = thin section, PAL = micropaleontology, DCP = close-up photo, and IW = interstitial water.
9. Consolidation (firmness): For a better visualization of the different intensities of sediment lithification, degrees of firmness are shown in the "Consolidation" column of the barrel sheets (Fig. F7). Firmness of recovered materials was defined according to Gealy et al. (1971). Five degrees of lithification were used:

   a. Extreme: Rock cannot be scratched or broken without the help of a saw.
   b. Strong: Rock breaks with difficulty. This includes hard, nonfriable, cemented, and/or compacted rock that is difficult or impossible to scratch with a fingernail or the edge of a spatula.
   c. Moderate: Hard but friable sediments can be broken easily or scratched with a spatula or a fingernail.
   d. Poor: Firm, cohesive, plastic sediment shows some resistance to finger pressure. This is common in clay-rich lithologies.
   e. Unlithified: Soft sediments have little strength and are readily deformed under the pressure of a fingernail or the broad blade of a spatula.

10. Facies: Nearly all of the facies described for sediments and rocks obtained during Leg 194 were formally presented as neritic (N), hemipelagic (H), or basement (B) on the barrel sheets. However,

in the "Lithologic Description" section many informal terms were used to describe facies and environments (e.g., deep shelf, reef, reef talus, proximal and distal slope, proximal and distal periplatform, sediment drift, open plateau, etc.).

11. Lithologic description: This section of the barrel sheet contains a written summary of the lithologies graphically presented. Leg 194 sedimentologists adopted the following format (Fig. F6):

    a. A principal name (written in capital letters) with modifiers, as discussed above, is placed just below the upper limit of each primary lithologic unit as defined by a contact graphic symbol.
    b. If an entire core consists of the same lithology, the principal name is then placed at the top of the "Description" column on the barrel sheet. When a core consists of thin (<10 cm) interbeds of distinctive lithology, or if the texture is intermediate between two types, two or more principal names separated by a slash can be used (e.g., skeletal grainstone/packstone).
    c. The color is listed directly beneath the principal name without using the Munsell Color Company (1994) color codes, as these are more accurately determined with the spectrophotometer (see "Core Physical Properties," p. 21).
    d. Directly beneath the color is the "General Description," where the lithologic unit is described. Dominant and supporting skeletal components are listed in order of importance as well as other distinctive observations that are not indicated graphically. Key features such as exposure surfaces, changes in mineralogy, sudden porosity changes, etc., are noted for emphasis where they are critical to identifying lithologic unit boundaries. The terminology for the thickness of sedimentary beds and laminae follows McKee and Weir (1953): very thick bedded (>100 cm), thick bedded (30–100 cm), medium bedded (10–30 cm), thin bedded (3–10 cm), thickly laminated (>0.3 cm), and thinly laminated (<0.3 cm).

Other Lithostratigraphy and Sedimentology Analyses

Smear Slides and Thin Sections

Tables summarizing data, such as grain size and relative abundance of sedimentary components from smear slides, were generated using a spreadsheet program (Sliders). Thin sections were analyzed using a Zeiss Axioplan microscope equipped with a digital camera. Digital photomicrographs were obtained, labeled, processed (sharpness, contrast, focus, etc.), and stored as TIF files. Observations were recorded on a customized spreadsheet.

Digital Camera Imagery

A track-mounted Kodak DCS 460 digital camera was set up in the core laboratory so that complete cores or specific sections of interest could be imaged, cataloged, and stored. Color hard copies were made available to ensure that both shifts could see images of the sediments and rocks that had been packed away and not available for their direct inspection. Additionally, these images were extremely useful for the site-report authors to review lithologies and to illustrate key features.

BIOSTRATIGRAPHY

Preliminary age assignments were based on planktonic foraminifer, calcareous nannofossil, and larger benthic foraminifer biostratigraphic analysis from core catcher samples, augmented by selected samples within cores to refine placement of datum levels and assemblage boundaries. Sample position, group abundance, group preservation, species frequency, and age or zone of each fossil group are recorded in the ODP database. The timescale and datum ages of planktonic foraminifers and nannofossils follow those of Berggren et al. (1995b). The larger benthic foraminiferal associations and ranges in northern Australia relative to Neogene planktonic foraminiferal zones as determined by Chaproniere (1981, 1984) and modified by Chaproniere and Betzler (1993) were also used.

Calcareous Nannofossils

Shipboard analysis focused primarily on the determination of key datum levels, which provided age control points. As many of the datums do not coincide with traditional zonal boundaries, it was more accurate and convenient to directly report the datums and their corresponding ages rather than translating them into fractional or multiple zones.

Smear slides were prepared directly from nonindurated sediments. For indurated or semi-indurated samples, a spatula was used to grind the samples and only the fine fractions were used to make slides. Slides were examined in a Zeiss light microscope at a magnification of 400× or 1000×, depending on the size of the nannofossils.

Calcareous nannofossil preservation was assessed using the following criteria:

G = good (little or no evidence of dissolution and/or overgrowth).
M = moderate (minor dissolution or crystal overgrowth observed).
P = poor (strong dissolution or crystal overgrowth; many specimens unidentifiable).

The total relative abundance of calcareous nannofossils for each sample was estimated as follows:

A = abundant (>50 specimens per field of view).
C = common (10–50 specimens per field of view).
F = few (1–10 specimens per field of view).
R = rare (1 specimen per 2 or more fields of view).

Nannofossil abundances of individual species were recorded as follows:

A = abundant (1–10 specimens per field of view).
C = common (1 specimen per 2–10 fields of view).
F = few (1 specimen per 11–50 fields of view).
R = rare (1 specimen per 51–200 fields of view).

Planktonic Foraminifers

The foraminifer-based ages were primarily determined by the use of the Berggren et al. (1995b) zonation scheme in association with the

tropical Neogene planktonic foraminifer "N-zonation" scheme of Blow (1969), with additional modifications by Kennett and Srinivasan (1983) and Bolli and Saunders (1985) (Fig. **F8**).

Sample preparation methods varied according to the degree of lithification. Most samples were ultrasonically agitated in a 10% hydrogen peroxide solution and were then washed over a <63-µm sieve. Semilithified samples were manually disaggregated into smaller pieces, sonicated, and sometimes heated in a 10% hydrogen peroxide solution. All samples were oven dried at ~60°C and then sieved into <1-mm, <250-µm, <150-µm, and >150-µm fractions. The <250-µm and <150-µm fractions were used for the examination of planktonic foraminifers. Planktonic foraminiferal abundances were quantitatively estimated using the following categories:

D = dominant (>30%).
A = abundant (>10%–30%).
F = few/frequent (>5%–10%).
R = rare (1%–5%).
P = present (<1%).
B = barren.

Preservation quality was described as follows:

G = good (>90% of specimens are well preserved and unbroken).
M = moderate (30%–90% of specimens with some dissolution damage such as etched and partially broken tests).
P = poor (high degree of fragmentation and encrustation).

The whole-sample fractional volume of planktonic foraminifers was described as follows:

A = abundant.
C = common.
F = few.
R = rare.
T = trace.

Benthic Foraminifers

Selected larger benthic foraminifers provided limited biostratigraphic resolution within platform intervals that lacked planktonic foraminifers and nannofossils. Larger foraminifers were identified at the genus level and, when possible, to species using washed core catcher samples supplemented by visual observation of half cores. Thin sections provided verification of generic and species-level identifications. Table **T3** provides the range estimates of selected taxa from Chaproniere (1981, 1984), modified by Chaproniere and Betzler (1993) and Betzler (1997). Betzler (1997) documented the extension of the upper range of *Lepidocyclina howchini* into the late Miocene on the Queensland Plateau. This range of *L. howchini* is in agreement with shipboard biostratigraphy provided by planktonic foraminifers and nannofossils in association with seismic stratigraphy. Detailed shore-based analysis of disaggregated specimens and thin sections will be required to document precisely the upper range of *L. howchini* on the Marion Plateau.

F8. Planktonic foraminifer ages, p. 47.

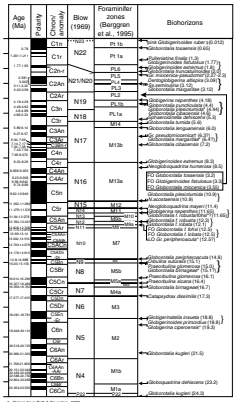

T3. Biostratigraphic ranges, p. 53.

Paleoenvironmental Analysis

Core catcher samples provided the principal source of data for paleoenvironmental interpretations. Lithologic variations necessitated the use of flexible preparation and analysis criteria. In lithified sections, interpretations were augmented by visual examination of whole cores and of thin sections prepared for sedimentological analysis (see "Lithostratigraphy and Sedimentology," p. 5).

Sample preparation methods varied according to the degree of lithification, as noted under "Planktonic Foraminifers," p. 12. Approximately 300 mg of sample was evenly distributed onto a black gridded picking tray and examined. The whole-sample fractional volume for principal constituents was described as follows:

D = dominant (major constituent).
A = abundant (>100 specimens).
C = common (>10–100 specimens).
R = rare (1–10 specimens).

Preservation quality was described as follows:

G = good (>90% of specimens are well preserved and unbroken).
M = moderate (30%–90% of specimens with some dissolution damage such as etched, recrystallized, and partially broken tests).
P = poor (high degree of fragmentation and encrustation).

Paleobathymetric estimates using benthic foraminifers utilized a modification of van Morkhoven et al.'s (1986) depth zonations to determine outer neritic and upper bathyal depths, and Hallock's (1999) zonations of larger benthic foraminifers (Table T4). The following bathymetric ranges were used:

IN = inner neritic (0–30 m).
MN = middle neritic (>30–100 m).
ON = outer neritic (>100–200 m).
UB = upper bathyal (>200 m).

All sites are in <400 m water depth. Inner and middle neritic depths were assumed to have been within the euphotic zone and were subdivided based upon the taxa and robustness of larger benthic foraminifers.

Depositional settings were interpreted based upon paleobathymetric (Table T4) and sediment constituent (Table T5) assessment. Platform environments were characterized by carbonate sedimentation in euphotic environments of inner to middle neritic depths, predominantly bryozoan–, red algal–, or coral-dominated facies and a significant component of larger benthic foraminifers. Periplatform environments were interpreted when carbonate bioclastic sediments of neritic origin dominated deposition in subeuphotic environments. Periplatform environments were further divided into "proximal" and "distal" based on the texture of the neritic constituents and the prevalence of sediments of pelagic origin. Proximal periplatform sediments are characterized by a wide size range of transported neritic material, generally with minor components of planktonic and outer neritic/upper bathyal benthic foraminifers. Distal periplatform sediments are characterized by silt to very fine sand-sized neritic carbonate debris mixed with planktonic foraminiferal tests and debris and conspicuous, although generally not abun-

T4. Benthic foraminifers, p. 54.

T5. Paleoenvironmental constituents and characteristics, p. 55.

dant, outer neritic to upper bathyal benthic foraminifers. Hemipelagic sediments are dominated by planktonic foraminiferal tests, with conspicuous outer neritic/upper bathyal benthic foraminifers. Terrigenous sediments, ranging from coarse quartz and lithic fragments to clays, are occasionally found in all depositional settings.

PALEOMAGNETISM

Paleomagnetic and rock magnetic investigations aboard the *JOIDES Resolution* during Leg 194 included routine measurements of natural remanent magnetization (NRM). Whole cores were measured before and after alternating-field (AF) demagnetization to 30 mT. Low-field magnetic susceptibility (k) measurements were made with the MST. NRM and a limited set of rock magnetic observations were made with discrete samples. A nonmagnetic APC core-barrel assembly was used for alternate cores in selected holes and the magnetic overprints in core recovered with this assembly were compared with those obtained with standard assemblies.

Measurement Procedure

The remanence measurements made during Leg 194 were conducted using the shipboard pass-through cryogenic magnetometer. The standard ODP magnetic coordinate system was used (+x = vertical upward from the split surface of archive halves, +y = left along split surface when looking upcore, and +z = downcore; see Fig. F9).

F9. Magnetic orientation convention, p. 48.

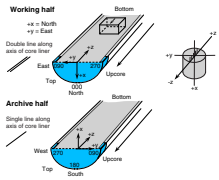

The output of the 2G magnetometer is given in magnetic moment in electromagnetic units with a background noise of ~10^{-7} gauss cm (SI 10^{-10} A/m^2). This gives an approximate limit for the intensity of magnetization that is required to reliably measure standard half- or whole-core samples, being ~10^{-6} A/m, or 0.001 mA/m. However, it should be noted that the magnetization of core liners can exceed this intensity. For standard discrete samples, the weakest measurable intensity is more than an order of magnitude greater than the long cores because of the smaller volume of material in the pickup coils.

NRM was initially measured on all archive-half sections. However, after comparisons between half-core and whole-core measurements revealed that core splitting sometimes induced significant overprints, whole cores were measured for the remainder of the leg. Core flow through the laboratory was modified with the long-core measurement being made before the MST run, which sped up processing significantly.

Long-core measurements were made at 5-cm intervals with 15-cm-long headers and trailers. Measurements at core and section ends and within intervals of drilling-related core deformation were removed during data processing. AF demagnetization was applied to cores at 30 mT and when time permitted, a 10-mT step was also measured.

Using the extrusion tool, discrete samples were collected from the working halves in standard 8-cm^3 plastic cubes. The discrete samples were analyzed with the shipboard pass-through cryogenic magnetometer using a tray designed for measuring six discrete samples at a time. To maintain ODP convention, the cube face with the arrow was placed downward on the tray. Samples were demagnetized by AF using the in-line demagnetizer installed on the pass-through cryogenic magnetometer. They were given anhysteretic remanent magnetizations and isothermal remanent magnetizations, and these were demagnetized to estab-

lish the magnetic characteristics of the recovered core. Magnetic susceptibility was measured for each whole-core section as part of the MST analysis (see "Core Physical Properties," p. 21). Susceptibility was measured on the MST using a Bartington MS2 meter coupled with a MS2C sensor coil with a diameter of 88 cm operating at 0.565 kHz. The sensor was set on SI units, and the data were stored in the Janus database in raw meter units. The sensor coil is sensitive over an interval of ~4 cm (half-power width of the response curve), and the width of the sensing region corresponds to a volume of 166 cm^3 of cored material. To convert to true SI volume susceptibilities, these values should be multiplied by 10^{-5} and then multiplied by a correction factor to take into account the volume of material that passed through the susceptibility coils. Except for measurements near the end of each section, the correction factor for a standard full ODP core is ~0.66 (= 1/1.5). The magnetic effect induced at the end of each core section was not corrected.

Core Orientation

During APC coring, full orientation was achieved with the Tensor multishot tool rigidly mounted onto a nonmagnetic sinker bar. The Tensor tool consists of three mutually perpendicular magnetic-field sensors and two perpendicular gravity sensors. The information from both sets of sensors allows the azimuth and dip of the hole to be measured, as well as the azimuth of the APC core double orientation line.

Magnetostratigraphy

Where magnetic cleaning successfully isolated the characteristic remanent magnetization, paleomagnetic inclinations were used to define magnetic polarity zones. On some occasions, it was possible to recover a satisfactory magnetic stratigraphy even when the inclination was of a single polarity because of a persistent overprint. On such occasions, the intensity and associated minor differences in inclination were used to extract the magnetostratigraphic signal. To recover the magnetostratigraphy, the persistent bias of the z-component was removed so that the alternating magnetic polarities required to define the magnetostratigraphic signal were made clearer. Interpretations of the magnetic polarity stratigraphy, with constraints from the biostratigraphic data, are presented in each of the site chapters. The revised timescale of Cande and Kent, as presented in Berggren et al. (1995a, 1995b), was used as a reference for the ages of Cenozoic polarity chrons.

Age Model

Age models, or continuous age-depth relationships, were constructed for Leg 194 sites to provide age estimates at any depth interval, particularly those of lithologic and seismic sequence boundaries. Age models also define significant changes in sedimentation rates. Calcareous nannofossil and planktonic foraminifer datums and ranges provided the age-depth control. Magnetostratigraphic control points, which were calibrated using the biostratigraphic results, were also considered. However, technical difficulties, poor core recovery, and abundant depositional hiatuses often prevented successful magnetostratigraphic interpretation.

The most common biostratigraphic datums are first occurrences (FO) or last occurrences (LO) of specific genera or species (see "Biostratigraphy," p. 12). An FO or LO datum cannot be observed in a particular sample, but must be interpreted to occur between two samples that define the interval of uncertainty for the true occurrence of the datum. Age controls are therefore plotted as depth intervals (error bars) extending from the top sample to the bottom sample. The symbol for the fossil type (calcareous nannoplankton or foraminifer) is plotted at the midpoint of the depth interval for graphical identification; however, the true LO or FO may occur anywhere in that interval in the absence of additional sampling.

In some cases, particularly at the top or bottom of a cored sediment sequence, an LO or FO datum cannot be defined, but the sample or samples contain age-diagnostic assemblages. In such cases, the known age range for the assemblage can be plotted as an age uncertainty interval for a particular sample or as an age-depth box for a series of samples. Age error bars (or age-depth boxes) should generally be plotted when the age uncertainty of a reference datum exceeds the time interval represented by the sample spacing. For instance, average sedimentation rates at Leg 194 sites range from 10 to 100 m/m.y., and the time interval represented by core catcher sample spacing (~10 m) is thus 1–10 m.y. This means that the core catcher sampling error is much larger (1–2 orders of magnitude) than the age errors of typical Cenozoic FO and LO datums (0.1–0.2 m.y.) In this case, plotting depth error bars is appropriate. However, for larger benthic foraminifer age control, used in carbonate platform sequences drilled on Leg 194, the age range for assemblages is substantial (millions of years) and age-depth boxes are used to plot the relatively loose but significant age-depth constraints.

When constructing the age model for a site, the depth error range for a datum also includes the uncertainty of where the sample came from in the drilled interval of a core. Recovered core segments are curated at the top of the cored interval and the nominal depth of a sample is defined in the curated space (see "Introduction," p. 1). If the recovered interval is shorter than the cored interval, the sample may originate from farther down in the section than implied by the nominal sample depth. In such cases, the depths of the bottom (downsection) samples of the datum depth intervals are corrected to the "bottom of cored interval" (BCI) (see datum tables in "Age Model" sections of the site chapters). This increases the depth interval of uncertainty to a more realistic interval, which may be up to 100% larger than the uncorrected one if recovery is limited to core catcher samples.

Age models were constructed by fitting straight line segments through the datum depth intervals. Rather than connecting midpoints of these depth intervals, straight lines were extended through as many control intervals as possible until a change in slope was necessary. Subsequent segments were fit so that changes in slope were minimal. This averaging procedure avoids introduction of artificial kinks (changes in sedimentation rates) in the age model that are not actually defined by the data but would result from low sampling resolution. The procedure was also used to define the duration of hiatuses by extrapolation of straight slope segments to the depth indicated by the physical expression of the hiatus, such as a hardground. The model thus becomes as simple, yet as accurate, as possible, reflecting the limitations of shipboard sampling.

Finally, sedimentation rates were computed and plotted, when appropriate, from the slopes of the straight line segments defining the age

models. These rates are averages of actual rates that may vary significantly over short, unresolved time intervals.

GEOCHEMISTRY

Inorganic Geochemistry

Interstitial Water Sampling and Chemical Analyses

The inorganic geochemistry program during Leg 194 was designed to provide rapid results to aid shipboard sampling and identification of key lithologic sections. The bulk of this shipboard program involved chemical analysis of interstitial waters and quantification of the chemistry and mineralogy of sediment samples.

Shipboard interstitial water analyses were performed on whole-round sections that were cut immediately after the core arrived on deck. The whole-round samples were usually taken from the lower third of every core that contained sufficient sediment for processing. After collection, the sediment was immediately extruded from the whole-round core liner and the surface was scraped to remove potentially contaminated exteriors. This sample was then placed into a titanium squeezer atop a filter previously rinsed in high-purity water to remove processing acids. Interstitial waters were retrieved by applying gradually increasing pressure to the squeezer up to a maximum pressure of 205 MPa (30,000 psi) using a hydraulic press (Manheim and Sayles, 1974). Interstitial water was collected through a 0.45-µm filter into a plastic syringe attached to the bottom of the squeezer assembly. Samples were filtered a second time through 0.45-µm polycarbonate filters and stored in plastic vials pending shipboard analyses. Aliquots for future shore-based analyses were placed in glass ampoules and were then heat sealed.

Interstitial water samples were routinely analyzed for salinity as total dissolved solids with a Goldberg optical handheld refractometer. The pH and alkalinity were determined by Gran titration with a Brinkmann pH electrode and a Metrohm autotitrator. Dissolved chloride was determined by titration with AgCl. Sodium, potassium, magnesium, calcium, and sulfate were analyzed by ion chromatography using a Dionex DX-100 ion chromatograph. Silica, phosphate, and ammonium concentrations were determined by wet chemical colorimetric methods and measured with a Milton Roy Spectronic 301 spectrophotometer following the analytical techniques described by Gieskes et al. (1991).

International Association of Physical Sciences Organizations (IAPSO) standard seawater was used for calibrating most techniques. The reproducibility of these analyses, expressed as 1-σ standard deviations of means of multiple determinations of a standard are alkalinity, <1.5%; chloride, <0.2%; calcium, <0.5%; magnesium, <0.5%; potassium, <2%; sulfate, ~1%; silica, <3%; phosphate, 4%; and ammonium, 4%. At all sites, sodium was determined using charge balance calculations, where

$$\Sigma_{\text{cation charge}} = \Sigma_{\text{anion charge}}.$$

Chemical data for interstitial waters are reported in molar units.

ICP-AES

Fe, Mn, B, Li, and Sr concentrations were determined by inductively coupled plasma–atomic emission spectroscopy (ICP-AES) following the general procedure outlined by Murray et al. (2000).

X-Ray Diffraction

Mineralogy was determined on solid carbonate samples using XRD analysis. Quantitative XRD analyses were performed on bulk samples to determine the relative percentage of aragonite, calcite, and dolomite. Samples were scanned from 15° to 35°2θ at 1°/min. To overcome the limitations of using multicomponent standards, conversion from peak areas to mineral weight percent was accomplished using the H-factor method of Hooten and Giorgeta (1977), modified to use low-magnesium calcite (LMC) as the common internal standard. In this method, the areas of the peaks of interest were obtained relative to the calcite peak and calibrated using calibration curves from a series of two-component standards. The final weight percent of each mineral was adjusted based on the total carbonate concentration measured on the same sample (see **"Organic Geochemistry,"** p. 19). In addition, the carbonate percentages were corrected for the presence of dolomite after the method described for Leg 133 (Shipboard Scientific Party, 1991). Overall, the accuracy of the XRD analysis is 5 wt% with a standard deviation of 3 wt%.

Organic Geochemistry

The shipboard organic geochemistry program included four routine sets of analyses. First, headspace analysis for volatile hydrocarbons was performed as required by ODP safety regulations. Second, elemental analyses of total carbon, carbonate carbon, total nitrogen, and total sulfur content of sediment samples (and calculation of total organic carbon) was performed. Third, organic matter type, quantity, and maturity were characterized using C/N ratios and Rock-Eval pyrolysis. Lastly, biomarker scans were performed on solvent-extractable organic matter fractions. Most of the procedures and instruments used are described by Emeis and Kvenvolden (1986) and generally are the same as those used during most recent ODP legs. Brief comments on routine sampling and deviations from standard practice are noted below; more detailed notes are presented in the "Explanatory Notes" chapters of ODP *Initial Reports* volumes for Legs 150, 156, 164, and 181 (Shipboard Scientific Party, 1994, 1995, 1996, 1999).

Volatile Hydrocarbons and Other Gases

Sediment-gas composition was determined on each core, primarily using the headspace sampling technique. For the headspace method, a cork borer was used to obtain a measured volume of sediment from the top of one section from each core immediately after retrieval. The sediment, with a typical volume of ~5 cm^3, was placed in a 21.5-cm^3 glass serum vial that was sealed with a septum and metal crimp cap. When consolidated or lithified samples were encountered, chips of material were placed in the vial and sealed. Before gas analysis, the vial was heated to 60°C for 30 min. A 5-cm^3 volume of the headspace gas was extracted from each vial using a glass syringe.

A Hewlett Packard 5890 Series II gas chromotagraph (GC) system was used for gas analysis. The Series II GC determines concentration of C_1 (methane), C_2 (ethane), and C_3 (propane) hydrocarbons with a flame ionization detector (FID). The chromatographic response was calibrated to standard gas mixtures.

Total Organic Carbon Content and Elemental Analyses

Total carbon, nitrogen, and sulfur contents of sediment samples were determined with a Carlo Erba Model NA1500 CNS analyzer. Approximately 6 mg of freeze-dried, ground sediment was combusted in oxygen at 1000°C. In this process, helium acts as a carrier gas, the oxygen is removed, and the combustion gases are reduced, separated by GC, and quantified with a thermal conductivity detector (TCD). Total organic carbon (TOC) content was calculated as the difference between total carbon (TC) and the inorganic (carbonate) carbon (IC) value generated by carbonate coulometry (i.e., TOC = TC – IC). We calculated C/S ratios assuming that all of the sulfur exists as pyrite within the sediments. C/S values <2 are generally considered representative of marine environments, whereas C/S values >5 indicate freshwater environments (Berner and Raiswell, 1984).

Organic Matter Characterization

Type and quality of organic matter in sediment were evaluated by Rock-Eval pyrolysis of hydrocarbons (Espitalié et al., 1986). In this procedure, volatile hydrocarbon content (in milligrams per gram of rock) released by heating at 300°C for 3 min is measured by the FID and labeled as an S_1 peak on the Rock-Eval pyrogram. Hydrocarbon quantity (in milligrams of hydrocarbon per gram of sediment) produced by pyrolysis as the temperature is increased from 300° to 600°C at a heating rate of 25°C/min is also measured by the FID and is called the S_2 peak. The nominal temperature at which the maximum rate of hydrocarbon yield is attained during S_2 analysis is the T_{max} value, which provides an estimate of organic matter thermal maturity, with values <435ºC indicative of immaturity relative to petroleum generation. The "oil window" is generally considered to range between T_{max} values of 435° and 465°C (Espitalié et al., 1986; Peters, 1986). CO_2 (in milligrams per gram), generated between 300° and 390°C, is measured using a TCD and is called the S_3 peak. TOC is calculated from S_1, S_2, and S_3, and from the oxidation of the remaining carbon in the sediment sample measured by a second TCD. The carbon-normalized hydrogen index (HI) (in milligrams of hydrocarbon per gram of carbon) and oxygen index (OI) (in milligrams of carbon dioxide per gram of carbon) are calculated from pyrolysis values by

$$HI = (100 \times S_2)/TOC \text{ and } OI = (100 \times S_3)/TOC.$$

The origin of sedimentary organic matter was further characterized using HI and organic carbon/nitrogen (C/N) values generated by the CNS analyzer. In general, high hydrogen index (>~200) and low oxygen index (<~150) values from Rock-Eval pyrolysis are indicative of marine (Type II) or lacustrine (Type I) organic matter. Furthermore, lacustrine organic matter generally shows higher HI and lower OI values than a marine counterpart (Espitalié et al., 1986; Peters, 1986). In addition, C/

N ratios of ~5–8 are generally considered to be indicative of marine organic matter (Bordovskiy, 1965; Emerson and Hedges, 1988; Meyers, 1994). In contrast, terrestrially derived organic matter from higher plants (Type III) exhibits relatively low HI (<~150) and relatively high OI values, and C/N ratios of ~25–35. Oxidized Type I and II organic matter may show HI and OI values similar to those obtained from Type III, and consistently low HI and OI values are characteristic of Type IV, or highly oxidized organic matter.

High Molecular Weight Hydrocarbons (Long-Chain Alkenones)

An attempt to identify long-chain alkenones in the sediments to estimate paleo–sea surface temperature (SST) was made. Solvent extract (bitumen) was obtained from 1 g of freeze-dried sediment by ultrasonic extraction with dichloromethane:methanol (99:1) for 30 min. The supernatant was pipetted into a vial, and the solvent was removed under a stream of nitrogen. The total extract was dissolved in 50 µL of hexane. A 1-µL aliquot was analyzed on a Hewlett Packard 6890 GC equipped with a 50 m × 0.2 mm HP Ultra 1 (crosslinked methyl silicon gum) capillary column (0.11-µm film thickness), tied to a Hewlett Packard 5973 mass selective detector. Operating conditions for the GC were as follows:

Splitless injection: injector temperature = 300°C and detector temperature = 320°C; and
Temperature program: 50°C (2 min), 20°C/min to 130°C, 4°C/min to 320°C (20 min), and 70°C/min to 50°C.

CORE PHYSICAL PROPERTIES

Physical properties measurements on Leg 194 provided

1. Near-continuous records for hole-to-hole correlation and construction of complete stratigraphic sequences and downhole log calibration;
2. Sediment properties (density, porosity, natural gamma radiation, magnetic susceptibility [MS], and color reflectance) for comparison with composition, diagenesis, and consolidation history and to help constrain the location of unconformities, sediment fracturing, and fluid migration and expulsion;
3. Data for the calculation of synthetic seismograms (i.e., *P*-wave velocity and bulk density) and integrated traveltime curves; and
4. Data for the calculation of local heat flow (downhole temperature and thermal conductivity).

Physical properties were measured on unsplit cores, on undisturbed parts of split cores, and on core plugs cut from the split cores. For rock cores (e.g., carbonate platform sediments and basement samples) the liners were split and the curated length of the whole cores was determined prior to MST measurement. The MST was used on whole cores and on some half-core sections (APC, XCB, and RCB) for nondestructive measurements of wet bulk density, *P*-wave velocity, MS, and natural gamma radiation. Because of their larger diameter relative to cores obtained with usual coring techniques, cores obtained using the ADCB were not ana-

lyzed with the MST. Thermal conductivity measurements were conducted on unsplit soft sediment cores and split rock cores. Three-directional *P*-wave velocities were measured on sediment and rock cores. Moisture content, wet and dry mass, and dry volume were measured from undisturbed samples of split cores, and bulk density, porosity, grain density, and void ratio were calculated. For samples of consolidated sediments, dry mass and wet and dry volume were determined to calculate the same suite of parameters.

To ensure thermal homogeneity for the physical properties measurements, the cores were allowed to come to thermal equilibrium at ambient room temperature (i.e., 22°–25°C). The first measurement station was the MST, which combines four sensors on an automated track. The sensors are the magnetic susceptibility loop (MSL), the gamma ray attenuation (GRA) bulk density, the *P*-wave logger (PWL), and the natural gamma radiation (NGR) detector. MST measurement intervals and periods for each core section were selected so that physical properties could be accurately characterized in 15 min for a 1.5-m-long section without hindering the flow of core processing through the laboratories. After MST analysis, thermal conductivity was measured on whole sediment cores. For rock cores, the cores were split prior to thermal conductivity measurements, and each measurement was conducted on half-core samples.

The working half of each section was used for further physical properties measurements of *P*-wave velocity, water content, and grain volume. Water content and grain volume were used to calculate bulk density, porosity, grain density, and related parameters. A summary of each of the physical properties measurement procedures for Leg 194 is outlined below. Blum (1997) provides a detailed description of the physical principles underlying the sampling methods.

MST Measurements

MS, bulk density, and NGR were generally measured on all cores that exceeded a minimum length of ~0.5 m regardless of the coring method. *P*-wave velocity was measured on all APC-cored intervals and some XCB- and RCB-cored intervals using the PWL.

In order to collect measurements, individual unsplit core sections were placed on the MST, which automatically moves the core section through the four sensors on a fiberglass boat. MST data are not continuous as a function of depth because of incomplete recovery, drilling-disturbed intervals, and removal of whole-round sections immediately after coring. The quality of these data are degraded in XCB and RCB sections where the core may be undersized with respect to the liner diameter and/or disturbed. Nevertheless, the general downhole trends are useful for stratigraphic correlations.

Magnetic Susceptibility Loop Sensor

High-amplitude MS is a function of the existence and concentration of ferro- and ferrimagnetic minerals such as magnetite, hematite, goethite, and titanomagnetite within sediment. The source of this material may be associated with the coarse sediment fraction of, for example, proximal turbidites and/or as single-domained magnetic material contained with the clay fraction. In the absence of ferro- and ferrimagnetic minerals, the MS is often of low amplitude induced by paramagnetic and diamagnetic minerals such as clays and evaporites. MS reflects

changes in magnetic mineralogy and, as a result, is widely used as a proxy for lithologic variations. MS is also used as a proxy for changes in composition that can be linked to lithologic changes and depositional processes.

The MSL was set to measure MS of unsplit core sections using a 5-cm sampling interval and a 4-s sampling period. MS is measured using a Bartington MS2 meter coupled to a MS2C sensor coil with a diameter of 88 cm operating at 565 Hz. The sensor is set to SI units, and data are stored in the ODP database in raw meter units. The sensor coil is sensitive over an interval of ~4 cm, and the width of the sensing region corresponds to a volume of 166 cm^3 of cored material. To convert to true SI volume susceptibilities, these values are multiplied first by 10^{-5} and then by a correction factor to take into account the volume of material that passed through the susceptibility coils. Except for measurements near the end of each section, the correction factor for a standard full ODP core is ~0.66. The diamagnetic contribution of the carbonates recovered during this leg reduced the value of weak field susceptibility in magnetic analysis because it biases the susceptibility. No correction was applied to the MS values for reduced core volume.

GRA Bulk Density

GRA bulk density was estimated for unsplit core sections and occasionally on half-core sections using the GRA sensor and a sampling period of 5 s every 5 cm. For each site, the GRA bulk density is an independent estimate at higher sampling resolution compared with the bulk density determined by the moisture and density (MAD) method. Measurement of GRA density is based on the principle that the attenuation, mainly by Compton scattering, of a collimated beam of gamma rays produced by a ^{137}Ce source passing through a known volume of sediment is related to material density (Evans, 1965).

P-Wave Velocity

The PWL measures *P*-wave velocity across the unsplit core sections using a sampling interval of 5 cm (4-s period). In order to determine the *P*-wave velocity, the PWL transmits 500-kHz *P*-wave pulses through the core at a frequency of 1 kHz. The transmitting and receiving transducers are aligned perpendicular to the core axis, and a pair of displacement transducers monitors the separation between the *P*-wave transducers. Variations in the outer diameter of the liner do not degrade the accuracy of the velocities, but the unconsolidated sediment or rock core must completely fill the liner for the PWL to provide acoustic coupling, which is often not the case with XCB and RCB cores. Measuring *P*-wave velocities on XCB and RCB cores, therefore, is not recommended. However, if the coupling is adequate, the measured velocities often provide an upper limit of the core velocity. Data quality is improved when the coupling between the liner and transducers is maintained by wetting the outside of the liner, which was not achieved during Leg 194. Overall, the resulting PWL data during Leg 194 have been seriously compromised.

Natural Gamma Radiation

As with MS, the NGR amplitude is a function of the terrigenous clay content within sediment. NGR emissions are a function of the random

and discrete decay of radioactive isotopes, predominantly those of U, Th, and K, and are measured through scintillating detectors arranged at 90° angles to each other and perpendicular to the core. NGR count typically correlates with increasing clay/shale content and/or diagenesis where uranium is sequestered from seawater and organic matter. Sand-prone and carbonate units usually tend to be characterized by low NGR counts. Ideally, these relationships can be used to define the location of shale-prone and sand-prone formations down the borehole. For siliciclastic units, shale and sand-prone units relate primarily to changes in relative sea level. In particular, coarsening-upward and fining-upward sedimentary sequences are expressed as overall decreasing and increasing NGR signatures, respectively. For carbonate units, lowstand systems tend to result in a decrease in carbonate production and deposition, thereby leading to sediment starvation and glauconite formation and deposition and the formation of hardgrounds.

NGR was measured for 5 s at 5-cm intervals. NGR calibration was performed at the beginning of the leg. For the interval at the top of the hole supported by the pipe, the maximum amplitude of the MST-NGR data was used to correct for the attenuation of the gamma ray wireline log data collected through the pipe.

Thermal Conductivity

Thermal conductivity was measured during Leg 194 using the TK04 system described by Blum (1997). This system employs a single-needle probe (Von Herzen and Maxwell, 1959), heated continuously, in full-space configuration for soft sediments and in half-space configuration for hard rock. The needle probe is a thin metal tube that contains a thermistor and a heater wire. The needle is assumed to be a perfect conductor because it is much more conductive than unconsolidated sediments. With this assumption, the temperature of the superconductive probe has a linear relationship with the natural logarithm of the time after the initiation of the heat:

$$T(t) = (q/4\pi k) \cdot ln(t) + C,$$

where T is the temperature, q is the heat input per unit length per unit time, k is the thermal conductivity, t is the time after the initiation of the heat, and C is a constant.

For full-space measurements, an aperture was drilled through the outer core liner and the 2 mm-diameter temperature probe inserted between the archive and working half of the core section. After insertion, the probe was heated at 3 W/m and the temperature rise was monitored. The optimal integration time for each conductivity measurement is calculated by an algorithm in the TK04 program.

Consolidated half-core rock specimens were measured for thermal conductivity using the half-space configuration. The needle probe was secured onto the flat surface of the half core. Good coupling with the needle probes was ensured by flattening and smoothing the core surface with carbide grit sandpaper. The samples and needles were then immersed in seawater for a minimum of 15 min prior to measurement.

The temperature analysis began once thermal stability of the sample had been established. Only when the background thermal drift was determined to be <0.04°C/min did the measurement process commence by activating the heater circuit and monitoring the temperature increase in the probe. This technique proved highly sensitive to small

variations in ambient temperature. In order to minimize this affect in the case of the half-core measurements, immersion in seawater kept the samples saturated, improved the thermal contact between the needle and the sample, and reduced thermal drift during measurement.

Thermal conductivity measurements were taken at a minimum frequency of one per core (usually Section 2) and at increased frequencies when time allowed. The reported thermal conductivity measurement for each sample was the average of three repeated measurements for the full-space method and four repetitions for the half-space method. Data are reported in W/(m·K) with a stated error of about 5% and precision of 2%. Variations in thermal conductivity are consistent with those in bulk density and porosity. A direct inverse relationship should exist between porosity (ϕ) and thermal conductivity because of the power law dependence of bulk thermal conductivity (K_{bulk}) on the solid matrix grain thermal conductivity (K_{grain}) and the thermal conductivity of the interstitial fluid (K_w) (Keen and Beaumont, 1990). This equation can be expressed as

$$K_{bulk} = K_w^{\phi} \cdot K_{grain}^{(1-\phi)}.$$

The observed relationship between the thermal conductivity and porosity can be compared with calculated bulk thermal conductivity using the measured porosity values and grain thermal conductivity values summarized in Table T6 (Keen and Beaumont, 1990).

T6. Thermal conductivity, p. 56.

Moisture and Density Measurements

MAD measurements (water content, wet and dry bulk density, grain density, and porosity) were routinely measured on unconsolidated sediment in 10-mL beakers and/or ~9.5-cm³ cubes cut from consolidated sediment and basement rocks. Both were sampled at a frequency of one per section. Sampling frequency was adjusted as needed to characterize all significant lithologies within a core. In XCB cores, which frequently showed a biscuiting-type disturbance, particular care was taken to sample undisturbed parts of the core and to avoid drilling slurry. Immediately after the beaker samples were collected, wet sediment mass (M_{wet}) was measured. For the sediment cubes, length, width, and height were measured with a SPI2000 caliper with an accuracy of 0.05 mm in order to calculate the wet bulk volume (V_{bulk}), which is equivalent to V_{wet} for the beaker calculation; V_{bulk} is the product of cube length, width, and height.

Dry sediment mass (M_{dry}) and dry sediment volume (V_{dry}) were measured after the beaker and sediment cube samples had dried in a convection oven for 24 hr at a temperature of 105° ± 5°C. After drying and prior to measuring dry mass and volume, the samples were stored in a desiccator for at least 1 hr to cool. Sample mass was determined to a precision of 0.01 g using two Scientech 202 electronic balances to compensate for the ship's motion. Grain volumes were determined using a helium Quantachrome Penta-Pycnometer with a precision of 0.02 cm³. The determination of water content followed the methods of the American Society for Testing and Materials (ASTM) designation (D) 2216 (ASTM, 1980). Blum (1997) discusses the fundamental phase relations and assumptions for the calculations of all relevant phase relationships summarized below:

1. Unconsolidated (beaker) sediment samples. The mass of the evaporated water (M_{water}) and the salt (M_{salt}) in the sample is given by

$$M_{water} = M_{wet} - M_{dry} \text{ and}$$

$$M_{salt} = M_{water}\,[s/(1-s)],$$

where s is the assumed saltwater salinity (0.035) corresponding to a pore-water density (ρ_{pw}) of 1.024 g/cm^3 and a salt density (ρ_{salt}) of 2.257 g/cm^3. The corrected mass of pore water (M_{pw}), volume of pore water (V_{pw}), mass of solids excluding salt (M_{solid}), volume of salt (V_{salt}), volume of solids excluding salt (V_{solid}) and the wet volume (V_{wet}) are, respectively,

$$M_{pw} = M_{water} + M_{salt} = M_{water}/(1-s),$$

$$V_{pw} = M_{pw}/\rho_{pw},$$

$$M_{solid} = M_{dry} - M_{salt},$$

$$V_{salt} = M_{salt}/\rho_{salt},$$

$$V_{solid} = V_{dry} - V_{salt} = V_{dry} - M_{salt}/\rho_{salt}, \text{ and}$$

$$V_{wet} = V_{solid} + V_{pw},$$

where M_{dry} and V_{dry} are the dry mass and volume that include the salt precipitated in the pores during the drying process.

2. Consolidated sediment cubes. For the consolidated sediment cubes, wet volume (V_{wet}) and wet mass (M_{wet}) are determined from

$$V_{pw} - V_{water} = V_{bulk} - V_{dry},$$

$$M_{pw} = V_{pw}\,\rho_{pw},$$

$$M_{salt} = M_{pw}\,s,$$

$$V_{salt} = M_{salt}/\rho_{salt},$$

$$V_{solid} = V_{dry} - V_{salt},$$

$$M_{water} = M_{pw}\,[(1 - s)/s],$$

$$V_{wet} - V_{bulk}, \text{ and}$$

$$M_{wet} = M_{dry} + M_{water}.$$

3. Calculation of MAD parameters. For all sediment samples (beakers and cubes), wet water content (w_{wet}) is expressed as the ratio of the mass of pore water to the wet sediment (total) mass, and the dry water content (w_{dry}) is the ratio of the mass of pore water to the mass of solids (excluding salt):

$$w_{wet} = M_{pw}/M_{wet} \text{ and}$$

$$w_{dry} = M_{pw}/M_{solid}.$$

In turn, bulk density (ρ_{wet}), dry bulk density (ρ_{dry}), sediment grain (solid) density (ρ_{solid}), porosity (ϕ), and void ratio (e) are calculated from

$$\rho_{wet} = M_{wet}/V_{wet},$$

$$\rho_{dry} = M_{solid}/V_{wet} \text{ or } M_{solid}/V_{bulk},$$

$$\rho_{solid} = M_{solid}/V_{solid},$$

$$\phi = V_{pw}/V_{wet}, \text{ and}$$

$$e = V_{pw}/V_{solid}.$$

Porosity-Depth Behavior

Porosity behavior as a function of depth is often described in terms of Athy's law (Athy, 1930). This empirical relationship presumes a negative exponential relationship between depth and porosity:

$$\phi(z) = \phi_o\, e^{-kz},$$

where $\phi(z)$ is the porosity as a function of depth z, ϕ_o is the surface porosity, and k controls the rate of decay of porosity with depth. A least-squares fit to this equation can be applied to estimate the surface porosity ϕ_o and the rate of decay of porosity. Variations from the general curve are often diagnostic of grain size and composition, facies variations, and interstitial fluid pressure disequilibrium.

P-Wave Velocities on Split Cores and Consolidated Samples

Velocity was measured using three pairs of perpendicularly oriented *P*-wave sensors (PWS1, PWS2, and PWS3). The method chosen for *P*-wave velocity measurements (V_P) was dependent on the degree of sediment consolidation. For unconsolidated sediments, the PWS1 (z-direction) and PWS2 (y-direction) insertion probe systems were used to measure the transverse (across the core axis) and longitudinal (along the core axis) *P*-wave velocity and seismic anisotropy. PWS1 and PWS2 transducer pairs, which have a fixed spacing of 7 cm (vertical) and 3.5 cm (horizontal), were inserted into the soft-sediment split cores. The PWS3 system uses a vertically oriented transducer pair that can be used with or without a liner correction. Alternatively, sample cubes or cylinders can also be measured. An acoustic signal of 500 kHz was transmitted and received by the two transducers. Analog to digital transformation of the signal allowed the seismic signal to be displayed on a digital oscilloscope so that the first-arrival waveform could be manually picked and velocity calculated. Zero traveltimes for the velocity transducers were measured using water (assumed to be at ambient temperature). To improve the coupling between the transducer and sample, distilled water was applied to the transducer/receiver heads. Measurements were

corrected for the additional traveltime required to pass through the core liner.

The measured velocities can be compared with the time-average equation of Wyllie et al. (1956), which states that the traveltime of an acoustic signal through rock is the sum of the traveltime through the solid matrix and the fluid phase:

$$1/V_{rock} = (1 - \phi)/V_{matrix} + \phi/V_{fluid}.$$

In general, the matrix is assumed to be calcite (V_{matrix} = 6530 m/s), and the pore fluid is assumed to be seawater (V_{fluid} = 1500 m/s). Often, the time-average equation provides a lower envelope for carbonate sediments. Deviations from the time-average equation are explained by different kinds of pore types (Anselmetti and Eberli, 1993). Moldic porosity shows a positive deviation from the time-average equation because the pores are integrated in a rigid framework. This type of porosity is common in the platform carbonates of the Leg 194 sites.

Anisotropy is determined using the difference between the average horizontal and vertical velocity using the following equation:

$$\text{Anisotropy} = 2(V_{Pt} - V_{Pl})/(V_{Pt} + V_{Pl}),$$

where V_{Pt} is the average transverse *P*-wave velocity and V_{Pl} is the longitudinal velocity. The velocity meter was calibrated by measuring V_P in distilled water. In unconsolidated sediments, at least one *P*-wave velocity measurement per section was made using one or both of the PWS1 and PWS2 systems.

Color Reflectance

Color was measured on split-core surfaces (of the archive half) using diffuse-reflected spectrophotometry. Light reflected from the material is collected in an integration sphere, normalized to the source light of the reflectance, and calibrated with the measurement of a pure white standard (100% reflection) and a black box (zero reflection) over the entire wavelength spectrum of visible light. Reflectance spectra are related to color using established international conventions. Shipboard reflectance was measured using an automated Minolta Photospectrometer (CM-2002) that measures the spectral reflectance of surfaces with a diameter of >8 mm. The instrument combines measurement, data processing, and display functions in a single unit. To ensure accuracy, the CM-2002 uses a double-beam feedback system, monitoring the illumination on the specimen at the time of measurement and automatically compensating for any changes in the intensity or spectral distribution of the light.

Color reflectance was measured on the archive halves of split cores to provide quantitative descriptions of sediment color. The color and variations in color can be used to interpret variations that occur within one core or between cores. A quantitative description allows the data to be analyzed in a formal manner and correlated with other data sets (e.g., NGR, carbonate content).

The two most common uses of color reflectance data are (1) color components such as L*a*b*, which provide detailed time series of relative changes in the composition of the bulk material and are frequently used to correlate sections from core to core or hole to hole and to ana-

lyze the cyclicity of lithologic changes, and (2) spectral data, which can be used to estimate the abundance of certain minerals. The first type of investigation, referred to as colorimetry, is simple and straightforward and is used for empirical correlations with other physical properties data and/or lithologic observations.

Color is reported using the L*a*b* system. It can be visualized as a cylindrical coordinate system in which the axis of the cylinder is the lightness component L*, ranging from 0% to 100%, and the radii are the chromaticity components a* and b*. Component a* is the green (negative) to red (positive) axis, and component b* is the blue (negative) to yellow (positive) axis. For Leg 194, the lightness (L*) component was used as a proxy for carbonate vs. terrigenous content, and the green–red component (a*) was used as a proxy for clay and glauconite concentration/variation within sediments.

In Situ Temperature Measurements

In situ temperature measurements were made using either an advanced piston core temperature (APCT) tool or a Davis-Villinger temperature probe (DVTP). The APCT tool fits directly into the coring shoe of the APC and consists of a battery pack, a data logger, and a platinum resistance temperature device calibrated over a temperature range from 0° to 30°C. Before entering the borehole, the tool was first briefly stopped at the mudline to thermally equilibrate with bottom water. After the APCT penetrated the sediment, it was held in place for 10 min and the APCT instrument recorded the temperature of the cutting shoe every 10 s. Initially, there was an instantaneous temperature rise due to frictional heating caused by APCT tool penetration, which gradually dissipates into the surrounding sediments. An equilibrium sediment temperature was then estimated by applying a mathematical heat-conduction model to the temperature decay record (Horai and Von Herzen, 1985). Additional information on the APCT tool can be found in Fisher and Becker (1993).

The DVTP tool is used in semilithified sediments, which the APCT tool cannot penetrate, and unlike the APCT, the DVTP requires a separate wireline run. This tool measures formation temperature using a probe that is pushed into the top of the sediment section. The probe is conical, with two thermistors, one located 1 cm from the tip of the probe and the other 12 cm above the tip. A third thermistor, referred to as the internal thermistor, is located in the electronics package. The thermistor is 1 mK in an operating range from –5° to 20°C, and the total operating range is –5° to 100°C. The thermistors were calibrated at the factory and on the laboratory bench before installation in the probe. In addition to the thermistors, the probe contains an accelerometer sensitive to 0.98 m/s^2. Both peak and mean acceleration are recorded by the logger. The accelerometer data are used to track disturbances to the instrument package during the equilibration interval.

For shallow-water sites, a longer mudline stop was required to ensure that the temperature tools had sufficient time to equilibrate to bottom-water temperatures. At deeper sites, this time was reduced as the tools were able to thermally equilibrate during descent through deeper waters with very low thermal gradients. This problem is less serious with the DVTP because it has a lower heat capacity and a thermal time constant that is less than that of the APCT tool.

Data reduction procedures are similar for both temperature tools. The synthetic thermal decay curves for the APCT and DVTP are a func-

tion of the geometry and thermal properties of the probe and the sediments (Bullard, 1954; Horai and Von Herzen, 1985). However, it is difficult to obtain a perfect match between the synthetic curves and the data because (1) the probe never reaches thermal equilibrium during the penetration period; (2) contrary to theory, the frictional pulse upon insertion is never instantaneous; and (3) temperature data are sampled at discrete intervals, meaning that the exact time of penetration is always uncertain. Thus, both the effective penetration time and equilibrium temperature must be estimated by applying a fitting procedure, which involves shifting the synthetic curves in time to obtain a match with the recorded data.

DOWNHOLE MEASUREMENTS

Logging Procedures and Logging Data

Introduction

Downhole logs reveal the physical, chemical, and structural properties of formations penetrated by a borehole. A variety of geophysical tools make rapid, continuous in situ measurements as a function of depth after the hole has been drilled that can be used to interpret the lithology of the penetrated formation. Where core recovery is good, core data are used to calibrate the geophysical signature of the rocks. In intervals of low core recovery or disturbed cores, log data may provide the only way to characterize the borehole section. Geophysical well logs can aid in characterizing sedimentary sequences and stratal stacking patterns when integrated with core and seismic reflection data.

Individual logging tools are joined together into tool strings (Fig. F10) so that several measurements can be made during each logging run (Table T7). The tool strings are lowered to the bottom of the borehole on a wireline cable, and data are logged as the tool string is pulled back up the hole. Repeat runs are made in some holes to improve coverage and confirm the accuracy of log data. Not all tool strings are run in each hole; refer to individual site chapters for details of logging strings deployed at each site.

Logging Tools and Tool Strings

During ODP Leg 194, the following three different logging strings were deployed (Fig. F10 and Table T7):

1. The triple combination (triple combo) string (resistivity, density, and porosity), which consists of the hostile environment spectral gamma ray sonde (HNGS), the phasor dual induction and spherically focused resistivity tool (DITE-SFR), the high temperature lithodensity tool (HLDT), and the accelerator porosity sonde (APS). The LDEO high-resolution temperature/acceleration/pressure tool (TAP) was attached at the bottom of this tool string. The LDEO multisensor gamma ray tool (MGT; Fig. F11) and the universal data telemetry module (UDTM) were included at the top of the tool string. The downhole switch in the UDTM allowed simultaneous deployment and proper cable lines switching between the MGT and Schlumberger tool string. This was the second test for the MGT after ODP Leg 191.

F10. Schematic illustration of tool string configurations. p. 49.

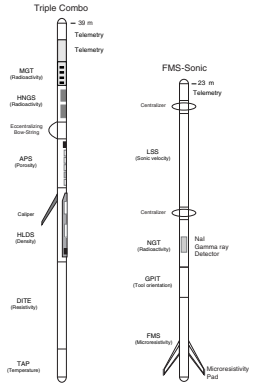

T7. Specifications of logging tools, p. 57.

F11. LDEO multisensor gamma ray tool, p. 50.

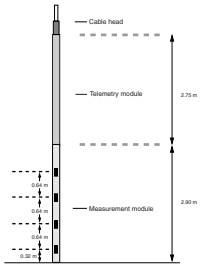

2. The FMS-sonic tool string, which consists of the Formation MicroScanner (FMS), the general purpose inclinometer tool (GPIT), and the dipole shear sonic imager (DSI). During Leg 194, the DSI was replaced by the long-spaced sonic tool (LSS) because of DSI tool failure. The natural gamma ray tool (NGT) was included between the LSS and the GPIT.
3. The well seismic tool (WST). Natural gamma ray data from the tools placed at the top of all but the WST tool string provide a reference log to correlate and depth shift several logging runs.

Principles and Uses of the Logging Tools

The parameter measured by each tool, the sample intervals used, and the vertical resolution, are summarized in Table T7. Explanations of tool name acronyms and their measurement units are summarized in Table T8.

T8. Logging tool acronyms and units of measurement, p. 58.

More detailed descriptions of individual logging tools and their geological applications can be found in Ellis (1987), Goldberg (1997), Lovell et al. (1998), Rider (1996), Schlumberger (1989, 1994), Serra (1984, 1986, 1989), and the Lamont-Doherty Earth Observatory–Borehole Research Group (LDEO-BRG) Wireline Logging Services Guide (1994).

Hostile Environment Spectral Gamma Ray Sonde and Natural Gamma Ray Tool

The HNGS and the NGT measure the natural gamma radiation from isotopes of potassium (K), thorium (Th), and uranium (U). The NGT uses a sodium-iodide (NaI) scintillation detector to measure the natural gamma ray emission and a five-window spectroscopy to determine concentrations of radioactive K (in weight percent), Th (in parts per million), and U (in parts per million). The HNGS uses a measurement principle similar to that of the NGT, but the HNGS uses two bismuth germanate scintillation detectors for gamma ray detection with full spectral processing, significantly improving tool precision compared to the NGT. The spectral analysis filters out gamma ray energies below 500 keV, eliminating sensitivity to bentonite or KCl in the drilling mud and improving measurement accuracy. The HNGS generates the same output as the NGT and also estimates the average borehole potassium contribution to the total potassium signal. Shipboard corrections to the HNGS account for variability in borehole size and borehole potassium concentrations. The NGT and HNGS also provide a measure of the total gamma ray signature SGR (gAPI [American Petroleum Institute] units) and uranium-free or computed gamma ray CGR (gAPI units).

The NGT response is influenced by the borehole diameter and the weight and concentration of bentonite or KCl present in the drilling mud. KCl may be added to the drilling mud to prevent freshwater clays from swelling and forming obstructions. All of these effects are corrected during processing of NGT data at LDEO-BRG.

Hostile Environment Lithodensity Sonde

The HLDS consists of a radioactive cesium (^{137}Cs) gamma ray source (622 keV) and far and near gamma ray detectors mounted on a shielded skid, which is pressed against the borehole wall by a hydraulically activated eccentralizing arm. Gamma rays emitted by the source experience both Compton scattering and photoelectric absorption. Compton scat-

tering involves the transfer of energy from gamma rays to the electrons in the formation via elastic collision. The number of scattered gamma rays that reach the detectors is directly related to the number of electrons in the formation, which is related to bulk density. Porosity may also be derived from this bulk density if the matrix density is known.

The HLDS also measures the photoelectric effect factor (PEF) caused by absorption of low-energy gamma rays. Photoelectric absorption occurs when gamma rays reach <150 keV after being repeatedly scattered by electrons in the formation. As PEF depends on the atomic number of elements in formation, it is essentially independent of porosity. Thus, PEF varies according to the chemical composition of the sediment. Some examples of PEF are: pure calcite = 5.08 barn/e^-; illite = 3.03 barn/e^-; quartz = 1.81 barn/e^-; and kaolinite = 1.49 barn/e^-. The PEF values can be used in combination with NGT curves to identify different types of clay minerals. Coupling between the tool and borehole wall is essential for good HLDS logs. Poor contact results in underestimation of density values. Both density correction and caliper measurement of the hole are used to check the contact quality.

Accelerator Porosity Sonde

The APS consists of a minitron neutron generator that produces fast neutrons (14.4 MeV) and five neutron detectors (four epithermal and one thermal) positioned at different spacings along the tool. The tool is pressed against the borehole wall by an eccentralizing bow-spring. Emitted high-energy (fast) neutrons are slowed down by collisions with atoms. The amount of energy lost per collision depends on the relative mass of the nucleus with which the neutron collides. A lot of energy loss occurs when the neutron strikes a nucleus of equal mass such as hydrogen, which is mainly present in pore water. Degrading to thermal energies (0.025 eV), the neutrons are captured by the nuclei of silicon, chlorine, and boron (Si, Cl, and B) and other elements resulting in a gamma ray emission. The neutron detectors record both the numbers of neutrons arriving at various distances from the source and the neutron arrival times, which act as a measure of formation porosity. However, hydrogen bound in minerals such as clays or in hydrocarbons also contributes to the measurement, so the raw porosity value is often an overestimate.

Dual Induction Tool and Spherically Focused Resistivity

The DITE provides three different measurements of electrical resistivities, each with a different depth of penetration into the formation. Two induction devices (deep and medium resistivity) transmit high-frequency alternating currents through transmitter coils, creating magnetic fields that induce secondary (Foucault) currents in the formation. These ground-loop currents produce new inductive signals, proportional to the conductivity of the formation, which are measured by the receiving coils. The measured conductivities are then converted to resistivity. A third device, a spherically focused resistivity instrument that gives higher vertical resolution, measures the current necessary to maintain a constant voltage drop across a fixed interval.

Multisensor Natural Gamma Ray Tool

The newly developed MGT was tested as part of the triple combo tool string (Fig. F10). The major advantage of the new tool is improved vertical resolution, comparable with the resolution of MST core measurements (Table T7). This is achieved by real-time stacking of natural gamma spectral data from four independent small-sized scintillation detectors positioned at 0.64-m spacing in the measurement module (Fig. F11). The tool provides 256-channel spectral analysis of each detector signal in the 0.2- to 3.0-MeV energy range. The full spectra are later combined into five- or three-window spectral data for compatibility with the older tools. The total gamma (gAPI) and concentrations of K (in weight percent), Th (in parts per million), and U (in parts per million) are calculated in real time either from spectral data of individual detectors or from stacked data. Postcruise processing will correct for borehole size and tool sticking, which is assessed by accelerator data recorded in the MGT.

High-Resolution Temperature/ Acceleration/Pressure Tool

The TAP is a "dual application" logging tool (i.e., it can operate as either a wireline tool or as a memory tool using the same sensors). Data acquisition electronics are dependent on the purpose and required precision of logging data. During Leg 194, the TAP was deployed as a memory tool in low-resolution mode with the data being stored in the tool and then downloaded after the logging run was completed.

Temperatures determined using the TAP do not necessarily represent in situ formation temperatures because water circulation during drilling will have disturbed temperature conditions in the borehole. However, from the spatial temperature gradient, abrupt temperature changes can be identified that may represent localized fluid flows into the borehole, indicating fluid pathways and fracturing and/or breaks in the temperature gradient that may correspond to contrasts in permeability at lithologic boundaries.

Long-Spaced Sonic Tool

The LSS measures the compressional wave velocity of the formation. The LSS is configured with two acoustic sources and two receivers, each spaced 61 cm apart. The spacing between the upper receiver pair and the transmitter pair is 2.44 m. The tool measures traveltime in microseconds over a certain distance in the formation. The configuration of the tool allows eight different traveltime measurements that compensate for irregular borehole walls. The velocity data together with the formation density can be used to generate a synthetic seismogram.

Formation MicroScanner Tool

The FMS produces high-resolution images of borehole wall microresistivity that can be used for detailed sedimentologic or structural interpretation. This tool has four orthogonally oriented pads, each with 16 button electrodes that are pressed against the borehole walls. Good contact with the borehole wall is necessary for acquiring good-quality data. Approximately 30% of a borehole with a diameter of 25 cm is imaged during a single pass. Coverage may be increased by a second run. The

vertical resolution of FMS images is ~5 mm, allowing features such as burrows, thin beds, fractures, veins, and vesicles to be imaged. The resistivity measurements are converted to color or grayscale images for display. In site chapters in this volume, local contrasts in all FMS figures were improved by applying dynamic normalization to the FMS data. A linear gain is applied, which keeps a constant mean and standard deviation within a sliding window of 1 m. When dynamic normalization is used, the values of color indicate relative changes in resistivity. Furthermore, the hole diameter was reduced artificially from 25.1 to 15.2 cm to reduce the blank space between the pad tracks and enlarge the FMS images proportionally.

FMS images are oriented to magnetic north using the GPIT (see "General Purpose Inclinometer Tool," p. 34). This allows the dip and strike of geological features intersecting the hole to be measured from processed FMS images. FMS images can be used to visually compare logs with the core to ascertain the orientations of bedding, fracture patterns, and sedimentary structures and to identify stacking patterns. FMS images have proved particularly valuable in interpreting sedimentary structures, and they have been used to identify cyclical stacking patterns in carbonates (Eberli, Swart, Malone, et al., 1997; Williams and Pirmez, 1999; Kroon et al., 2000), turbidite deposits (Lovell et al., 1998), and facies changes (Serra, 1989).

General Purpose Inclinometer Tool

The GPIT is included in the FMS-sonic tool string to calculate tool acceleration and orientation during logging. The GPIT contains a triple-axis accelerometer and a triple-axis magnetometer. The GPIT records the orientation of the FMS images and allows more precise determination of log depths than can be determined from cable length, which may experience stretching and/or be affected by ship heave.

Well Seismic Tool

The WST is used to produce a zero-offset vertical seismic profile and/or check shots in the borehole. The WST consists of a single geophone used to record the full waveform of acoustic waves generated by a seismic source positioned just below the sea surface. During Leg 194, a 300-in^3 air gun, positioned at a water depth of ~7 m with a borehole offset of 49 m on the port side of the *JOIDES Resolution,* was used as the seismic source. The WST was clamped against the borehole wall at 30- to 50-m intervals, and the air gun was typically fired between 5 and 15 times at each station. The recorded waveforms were stacked and a one-way traveltime was determined from the median of the first breaks for each station, thus providing check shots for calibration of the integrated transit time calculated from sonic logs. Check shot calibration is required for the core-seismic correlation because *P*-wave velocities derived from the sonic log may differ significantly from true formation velocity because of (1) frequency dispersion (the sonic tool operates at 10–20 kHz, with seismic data in the 50–200 Hz range), (2) difference in travel paths between well seismic and surface seismic surveys, and (3) borehole effects caused by formation alterations (Schlumberger, 1989). In addition, sonic logs cannot be measured through pipe, so the traveltime down to the uppermost logging point has to be estimated by other means.

Drill String Acceleration Tool

The drill string acceleration (DSA) tool is a modular downhole tool designed to acquire acceleration and pressure data near the bit. The DSA tool contains a single-axis high-sensitivity accelerometer for heave measurements, a three-axial high-frequency accelerometer for drill bit vibrations, and a high-resolution pressure sensor. For ease of deployment, the DSA tool has been designed as a removable extension of the APC/XCB/RCB and HYACE core barrels. Using standard threaded connections, the DSA tool was attached to the top of the rotary HYACE core barrel, without affect coring activities.

On each run, the DSA tool begins data acquisition at a predetermined depth as programmed by the LDEO logger. In addition to drilling vibration data and downhole pipe motion data, information about core barrel landing, pressure up, and other operational events are recorded by the DSA tool to assist in development of the HYACE core barrels. Upon DSA/core barrel retrieval, the DSA tool is disconnected and the data downloaded to the third party data acquisition system in the DHML for immediate analysis.

Data Quality

Logging data quality may be seriously degraded by rapid changes in the hole diameter and in sections where the borehole diameter greatly decreases or is washed out.

Deep-investigation measurements such as resistivity and sonic velocity are least sensitive to borehole conditions. Nuclear measurements (density and neutron porosity) are more sensitive because of their shallower depth of investigation and the effect of drilling fluid volume on neutron and gamma ray attenuation. Corrections can be applied to the original data in order to reduce these effects. Very large washouts, however, cannot be corrected for. HNGS and NGT data provide a depth correlation between logging runs. Logs from different tool strings may, however, still have minor depth mismatches caused by either cable stretch or ship heave during recording. Ship heave is minimized by a hydraulic wireline heave compensator designed to adjust for rig motion during logging operations.

Data Recording and Processing

Data for each logging run were recorded and stored digitally and monitored in real time using the Schlumberger MAXIS 500 system. After logging at each hole, data were transferred to the shipboard downhole measurements laboratory for preliminary processing and interpretation. FMS image data were interpreted using Schlumberger's Geoframe 3.8 software package. Well seismic, sonic, and density data were used for calculation of synthetic seismograms with GeoQuest's IESX software package to establish the seismic to borehole tie.

Log data were also transmitted to LDEO-BRG using a FFASTEST satellite high-speed data link for processing soon after each hole was logged. Data processing at LDEO-BRG consists of (1) depth-shifting all logs relative to a common datum (i.e., mbsf), (2) corrections specific to individual tools, and (3) quality control and rejection of unrealistic or spurious values. Once processed at LDEO-BRG, log data were transmitted back to the ship providing near real-time data processing. Log curves of LDEO-BRG-processed data were then replotted on board (see the "Downhole

Measurements" section in each site chapter). Further postcruise processing of the log data from the FMS is performed at LDEO-BRG.

Postcruise-processed acoustic, caliper, density, gamma ray, neutron porosity, resistivity, and temperature data in ASCII format are available directly from the LDEO-BRG Internet Web site at **http://www.ldeo.columbia.edu/BRG/ODP/DATABASE/**. A summary of "logging highlights" is posted on the LDEO-BRG Web site at the end of each leg.

Downhole logging aboard the *JOIDES Resolution* is provided by LDEO-BRG in conjunction with Leicester University Borehole Research, the Laboratoire de Mesures en Forages Montpellier, University of Aachen, University of Tokyo, and Schlumberger Well Logging Services.

REFERENCES

Anselmetti, F.S., and Eberli, G.P., 1993. Controls on sonic velocity in carbonates. *Pure Appl. Geophys.,* 141:287–323.

ASTM, 1980. Standard method for laboratory determination of water (moisture) content of soil, rock and soil-aggregate mixtures. In *Annual Book of ASTM Standards:* Philadelphia (Am. Soc. Testing and Mater.).

Athy, L.F., 1930. Density, porosity, and compaction of sedimentary rocks. *AAPG Bull.,* 14:1–24.

Berggren, W.A., Hilgen, F.J., Langereis, C.G., Kent, D.V., Obradovich, J.D., Raffi, I., Raymo, M.E., and Shackleton, N.J., 1995a. Late Neogene chronology: new perspectives in high-resolution stratigraphy. *Geol. Soc. Am. Bull.,* 107:1272–1287.

Berggren, W.A., Kent, D.V., Swisher, C.C., III, and Aubry, M.-P., 1995b. A revised Cenozoic geochronology and chronostratigraphy. *In* Berggren, W.A., Kent, D.V., Aubry, M.-P., and Hardenbol, J. (Eds.), *Geochronology, Time Scales and Global Stratigraphic Correlation.* Spec. Publ.—Soc. Econ. Paleontol. Mineral. (Soc. Sediment. Geol.), 54:129–212.

Berner, R.A., and Raiswell, R., 1984. C/S method for distinguishing freshwater from marine sedimentary rocks. *Geology,* 12:365–368.

Betzler, C., 1997. Ecological control on geometries of carbonate platforms: Miocene/Pliocene shallow-water microfaunas and carbonate biofacies from the Queensland Plateau (NE Australia). *Facies,* 37:147–166.

Blow, W.H., 1969. Late middle Eocene to Recent planktonic foraminiferal biostratigraphy. *In* Brönnimann, P., and Renz, H.H. (Eds.), *Proc. First Int. Conf. Planktonic Microfossils, Geneva, 1967:* Leiden (E.J. Brill), 1:199–422.

Blum, P., 1997. Physical properties handbook: a guide to the shipboard measurement of physical properties of deep-sea cores. *ODP Tech. Note,* 26 [Online]. Available from World Wide Web: <http://www-odp.tamu.edu/publications/tnotes/tn26/INDEX.HTM>. [Cited 2001-01-10]

Bolli, H.M., and Saunders, J.B., 1985. Oligocene to Holocene low latitude planktic foraminifera. *In* Bolli, H.M., Saunders, J.B., and Perch-Nielsen, K. (Eds.), *Plankton Stratigraphy:* Cambridge (Cambridge Univ. Press), 155–262.

Bordovskiy, O.K., 1965. Accumulation and transformation of organic substances in marine sediment, 2. Sources of organic matter in marine basins. *Mar. Geol.,* 3:5–31.

Bullard, E.C., 1954. The flow of heat through the floor of the Atlantic Ocean. *Proc. R. Soc. London A,* 222:408–429.

Cande, S.C., and Kent, D.V., 1995. Revised calibration of the geomagnetic polarity timescale for the Late Cretaceous and Cenozoic. *J. Geophys. Res.,* 100:6093–6095.

Chaproniere, G.C.H., 1981. Australasian mid-Tertiary larger foraminiferal associations and their bearing on the East Indian Letter Classification. *BMR J. Aust. Geol. Geophys.,* 6:145–151.

————, 1984. The Neogene larger foraminiferal sequence in the Australian and New Zealand regions, and its relevance to the East Indian Letter Stage classification. *Palaeogeogr., Palaeoclimatol., Palaeoecol.,* 46:25–35.

Chaproniere, G.C.H., and Betzler, C., 1993. Larger foramineral biostratigraphy of Sites 815, 816, and 826, Leg 133, northeastern Australia. *In* McKenzie, J.A., Davies, P.J., Palmer-Julson, A., et al., *Proc. ODP, Sci. Results,* 133: College Station, TX (Ocean Drilling Program), 39–49.

Droser, M.L., and Bottjer, D.J., 1986. A semiquantitative field classification of ichnofabric. *J. Sediment. Petrol.,* 56:558–559.

Dunham, R.J., 1962. Classification of carbonate rocks according to depositional texture. *In* Ham, W.E. (Ed.), *Classification of Carbonate Rocks.* AAPG Mem., 108–121.

Eberli, G.P., Swart, P.K., Malone, M.J., et al., 1997. *Proc. ODP, Init. Repts.,* 166: College Station, TX (Ocean Drilling Program).

Ellis, D.V., 1987. *Well Logging for Earth Scientists:* New York (Elsevier).

Embry, A.F., and Klovan, J.E., 1971. A late Devonian reef tract on northeastern Banks Island, Northwest Territories. *Bull. Can. Pet. Geol.,* 19:730–781.

Emeis, K.-C., and Kvenvolden, K.A., 1986. Shipboard organic geochemistry on *JOIDES Resolution. ODP Tech. Note,* 7.

Emerson, S., and Hedges, J.I., 1988. Processes controlling the organic carbon content of open ocean sediments. *Paleoceanography,* 3:621–634.

Espitalié, J., Deroo, G., and Marquis, F., 1986. La pyrolyse Rock-Eval et ses applications, Partie III. *Rev. Inst. Fr. Pet.,* 41:73–89.

Evans, H.B., 1965. GRAPE—a device for continuous determination of material density and porosity. *Trans. SPWLA 6th Ann. Logging Symp.,* Dallas, 2:B1–B25.

Fisher, A., and Becker, K., 1993. A guide to ODP tools for downhole measurements. *ODP Tech. Note,* 10.

Gealy, E.L., Winterer, E.L., and Moberly, R., Jr., 1971. Methods, conventions, and general observations. *In* Winterer, E.L., Riedel, W.R., et al., *Init. Repts. DSDP,* 7 (Pt. 1): Washington (U.S. Govt. Printing Office), 9–26.

Gieskes, J.M., Gamo, T., and Brumsack, H., 1991. Chemical methods for interstitial water analysis aboard *JOIDES Resolution. ODP Tech. Note,* 15.

Goldberg, D., 1997. The role of downhole measurements in marine geology and geophysics. *Rev. Geophys.,* 35:315–342.

Hallock, P., 1999. Symbiont-bearing foraminifera. *In* Sen Gupta, B.K., *Modern Foraminifera:* Amsterdam (Kluwer), 123–149.

Hooton, D.H., and Giorgetta, N.E., 1977. Quantitative X-ray diffraction analysis by a direct calculation method. *X-Ray Spectrom.,* 6:2–5.

Horai, K., and Von Herzen, R.P., 1985. Measurement of heat flow on Leg 86 of the Deep Sea Drilling Project. *In* Heath, G.R., Burckle, L.H., et al., *Init. Repts. DSDP,* 86: Washington (U.S. Govt. Printing Office), 759–777.

Keen, C., and Beaumont, C., 1990. Geodynamics of rifted continental margins. *In* Keen, M.J., and Williams, G.L. (Eds.), *Geology of the continental margin of Eastern Canada,* Geol. Soc. Am, 1:391–472.

Kennett, J.P., and Srinivasan, M.S., 1983. *Neogene Planktonic Foraminifera: A Phylogenetic Atlas:* Stroudsburg, PA (Hutchinson Ross).

Kroon, D., Williams, T., Pirmez, C., Spezzaferri, S., Sato, T., and Wright, J.D., 2000. Coupled early Pliocene–middle Miocene bio-cyclostratigraphy of Site 1006 reveals orbitally induced cyclicity patterns of Great Bahama Bank carbonate production. *In* Swart, P.K., Eberli, G.P., Malone, M.J., and Sarg, J.F. (Eds.), *Proc. ODP, Sci. Results,* 166: College Station TX (Ocean Drilling Program), 155–166.

Lamont-Doherty Earth Observatory–Borehole Research Group, 1994. *Wireline Logging Services Guide*: Lamont-Doherty Earth Observatory–Borehole Research Group.

Lovell, M.A., Harvey, P.K., Brewer, T.S., Williams, C., Jackson, P.D., and Williamson, G., 1998. Application of FMS images in the Ocean Drilling Program: an overview. *In* Cramp, A., MacLeod, C.J., Lee, S.V., and Jones, E.J.W. (Eds.), *Geological Evolution of Ocean Basins: Results from the Ocean Drilling Program.* Spec. Publ.—Geol. Soc. London, 131:287–303.

Manheim, F.T., and Sayles, F.L., 1974. Composition and origin of interstitial waters of marine sediments, based on deep sea drill cores. *In* Goldberg, E.D. (Ed.), *The Sea* (Vol. 5): *Marine Chemistry: The Sedimentary Cycle:* New York (Wiley), 527–568.

McKee, E.D., and Weir, G.W., 1953. Terminology for stratification and cross-stratification in sedimentary rocks. *Geol. Soc. Am. Bull.,* 64:381–390.

Meyers, P.A., 1994. Preservation of elemental and isotopic source identification of sedimentary organic matter. *Chem. Geol.,* 144:289–302.

Munsell Color Company, Inc., 1994. *Munsell Soil Color Chart:* (Revised ed.): Newburgh, MD (Munsell Color).

Murray, R.W., Miller, D.J., and Kryc, K.A., 2000. Analysis of major and trace elements in rocks, sediments, and interstitial waters by inductively coupled plasma–atomic emission spectrometry (ICP-AES). *ODP Tech. Note,* 29 [Online]. Available from World

Wide Web: <http://www-odp.tamu.edu/publications/tnotes/tn29/INDEX.HTM>. [Cited 2001-01-10]

Peters, K.E., 1986. Guidelines for evaluating petroleum source rock using programmed pyrolysis. *AAPG Bull.,* 70:318–329.

Rider, M., 1996. *The Geological Interpretation of Well Logs* (2nd ed.): Caithness (Whittles Publishing).

Schlumberger, 1989. *Log Interpretation Principles/Applications:* Houston (Schlumberger Educ. Services), SMP–7017.

————, 1994. *IPL Integrated Porosity Lithology:* Houston (Schlumberger Wireline and Testing), SMP-9270.

Serra, O., 1984. *Fundamentals of Well-Log Interpretation* (Vol. 1): *The Acquisition of Logging Data:* Dev. Pet. Sci., 15A.

————, 1986. *Fundamentals of Well-Log Interpretation* (Vol. 2): *The Interpretation of Logging Data*. Dev. Pet. Sci., 15B.

————, 1989. *Formation MicroScanner Image Interpretation:* Houston (Schlumberger Educ. Services), SMP-7028.

Shepard, F., 1954. Nomenclature based on sand-silt-clay ratios. *J. Sediment. Petrol.,* 24:151–158.

Shipboard Scientific Party, 1991. Explanatory notes. *In* Davies, P.J., McKenzie, J.A., Palmer-Julson, A., et al., *Proc. ODP, Init. Repts.,* 133 (Pt. 1): College Station, TX (Ocean Drilling Program), 31–58.

————, 1992. Explanatory notes. *In* Mayer, L., Pisias, N., Janeck, T., et al., *Proc. ODP, Init. Repts.,* 138 (Pt. 1): College Station, TX (Ocean Drilling Program), 13–42.

————, 1994. Explanatory notes. *In* Mountain, G.S., Miller, K.G., Blum, P., et al., *Proc. ODP, Init. Repts.,* 150: College Station, TX (Ocean Drilling Program), 21–42.

————, 1995. Explanatory notes. *In* Shipley, T.H., Ogawa, Y., Blum, P., et al., *Proc. ODP, Init. Repts.,* 156: College Station, TX (Ocean Drilling Program), 39–68.

————, 1996. Explanatory notes. *In* Paull, C.K., Matsumoto, R., Wallace, P.J., et al., *Proc. ODP, Init. Repts.,* 164: College Station, TX (Ocean Drilling Program), 13–41.

————, 1999a. Explanatory notes. *In* Gersonde, R., Hodell, D.A., Blum, P., et al., *Proc. ODP, Init. Repts.,* 177, 1–57 [CD-ROM]. Available from: Ocean Drilling Program, Texas A&M University, College Station, TX 77845-9547, U.S.A.

————, 1999b. Explanatory notes. *In* Carter, R.M., McCave, I.N., Richter, C., Carter, L., et al., *Proc. ODP, Init. Repts*. 181, 1–65 [CD-ROM]. Available from: Ocean Drilling Program, Texas A&M University, College Station TX 77845-9547, U.S.A.

————, 2000. Explanatory notes. *In* Wang, P., Prell, W.L., Blum, P., et al., *Proc. ODP, Init. Repts.,* 184, 1–48 [CD-ROM]. Available from: Ocean Drilling Program, Texas A&M University, College Station TX 77845-9547, USA.

Tucker, M.E., and Wright, P.V., 1990. *Carbonate Sedimentology:* Oxford (Blackwell Sci. Publ.).

van Morkhoven, F.P.C.M., Berggren, W.A., and Edwards, A.S., 1986. Cenozoic cosmopolitan deep-water benthic foraminifera. *Bull. Cent. Rech. Explor.—Prod. Elf-Aquitaine,* 11.

Von Herzen, R.P., and Maxwell, A.E., 1959. The measurement of thermal conductivity of deep-sea sediments by a needle-probe method. *J. Geophys. Res.,* 64:1557–1563.

Wentworth, C.K., 1922. A scale of grade and class terms of clastic sediments. *J. Geol.,* 30:377–392.

Williams, T., and Pirmez, C., 1999. FMS images from carbonates of the Bahama Bank Slope, ODP Leg 166: lithological identification and cyclostratigraphy. *In* Lovell, M.A., Williamson, G., and Harvey, P.K. (Eds.), *Borehole Imaging: Application and Case Histories*. Spec. Publ.—Geol. Soc. London, 159:227–238.

Wyllie, M.R.J., Gregory, A.R., and Gardner, L.W., 1956. Elastic wave velocities in heterogeneous and porous media. *Geophysics,* 21:41–70.

Figure F1. Graphic symbols (used during Leg 194) for the three main sediment and rock categories and for basement.

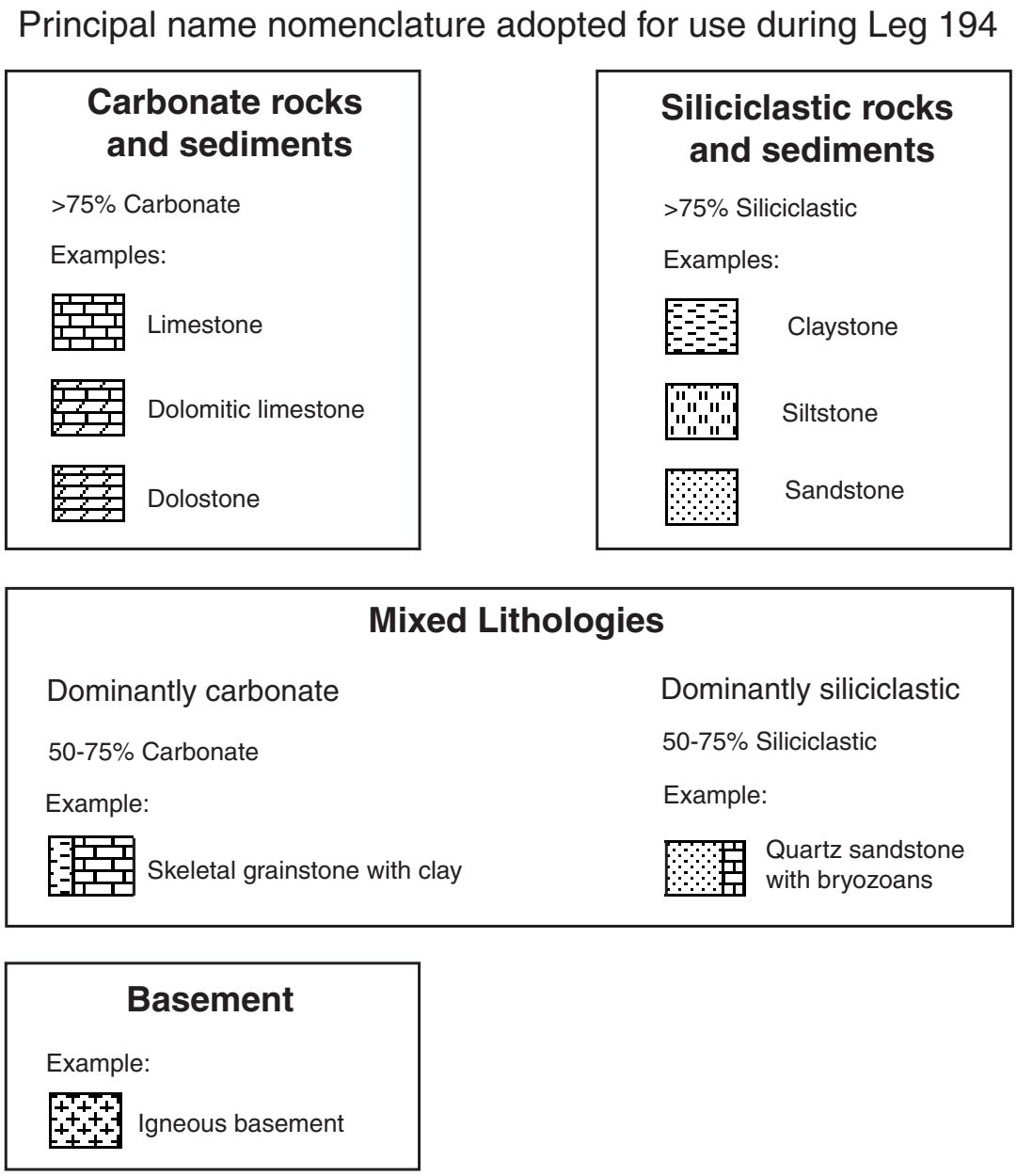

Figure F2. The Dunham (1962) classification of limestones according to depositional texture, as modified by Embry and Klovan (1971).

<table>
<tr><td colspan="6">Allochthonous limestone
original components not organically
bound during deposition</td><td colspan="3">Autochthonous limestone
original components organically
bound during deposition</td></tr>
<tr><td colspan="4">Less than 10% >2 mm components</td><td colspan="2">Greater than
10% >2 mm
components</td><td colspan="3">Boundstone</td></tr>
<tr><td colspan="3">Contains lime mud (<0.02 mm)</td><td>No
lime
mud</td><td rowspan="3">Matrix
supported</td><td rowspan="3">>2 mm
component
supported</td><td rowspan="3">By
organisms
which
act as
barriers</td><td rowspan="3">By
organisms
which
encrust
and
bind</td><td rowspan="3">By
organisms
which
build
a rigid
framework</td></tr>
<tr><td colspan="2">Mud supported</td><td colspan="2" rowspan="2">Grain
supported</td></tr>
<tr><td>Less than
10% grains
(>0.02 mm
to <2 mm)</td><td>Greater
than
10%
grains</td></tr>
<tr><td>Mudstone</td><td>Wackestone</td><td>Packstone</td><td>Grainstone</td><td>Floatstone</td><td>Rudstone</td><td>Bafflestone</td><td>Bindstone</td><td>Framestone</td></tr>
</table>

Figure F3. Udden-Wentworth grain-size classification of terrigenous sediments (from Wentworth, 1922).

Millimeters (mm)	Micrometers (μm)	Phi (ϕ)	Wentworth size class		Rock type
4096		-12.0	Boulder		
256		-8.0	Cobble	Gravel	Conglomerate/ Breccia
64		-6.0	Pebble		
4		-2.0	Granule		
2.00		-1.0	Very coarse sand		
1.00		0.0	Coarse sand		
1/2 0.50	500	1.0	Medium sand	Sand	Sandstone
1/4 0.25	250	2.0	Fine sand		
1/8 0.125	125	3.0	Very fine sand		
1/16 0.0625	63	4.0	Coarse silt		
1/32 0.031	31	5.0	Medium silt		
1/64 0.0156	15.6	6.0	Fine silt	Silt	Siltstone
1/128 0.0078	7.8	7.0	Very fine silt		
1/256 0.0039	3.9	8.0			
0.00006	0.06	14.0	Clay	Mud	Claystone

Figure F4. Diagram showing the classification scheme used for siliciclastic sediments and rocks (after Shepard, 1954).

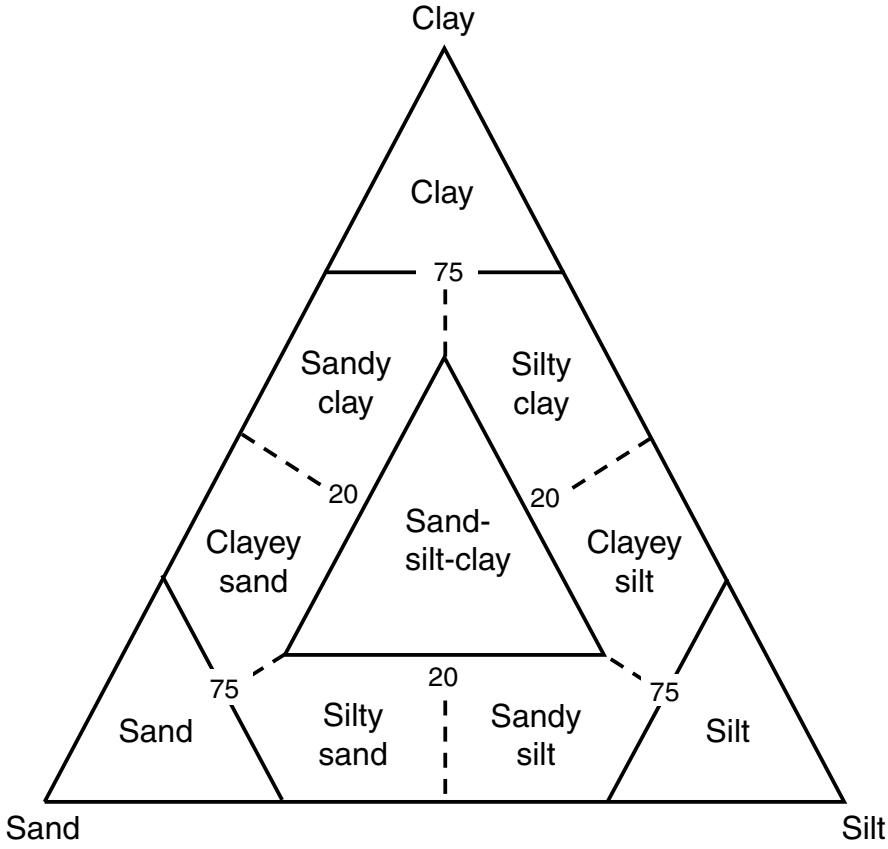

Figure F5. The visual core description (VCD) sheet developed and used by sedimentologists during Leg 194.

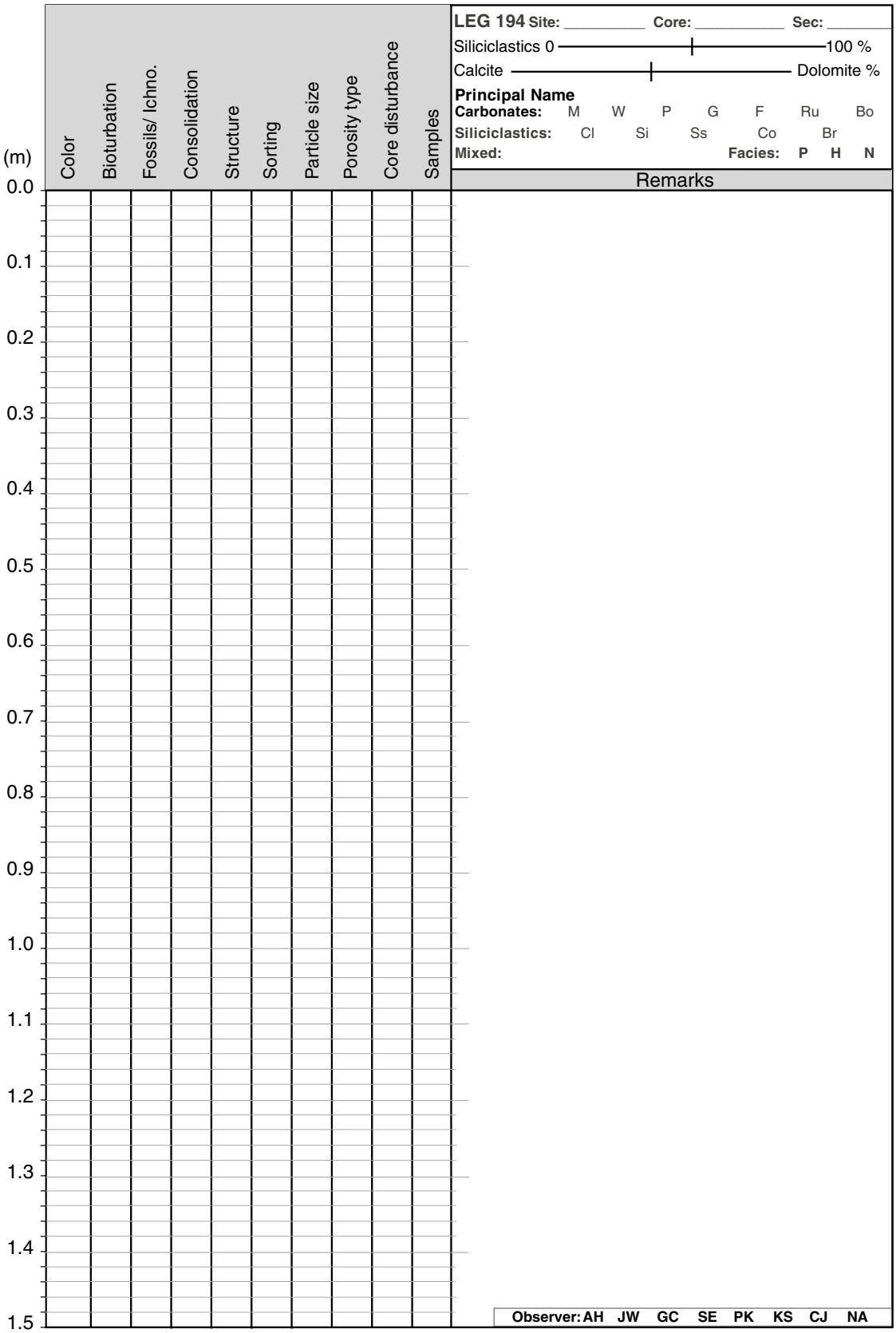

Figure F6. A completed core description form as used during Leg 194.

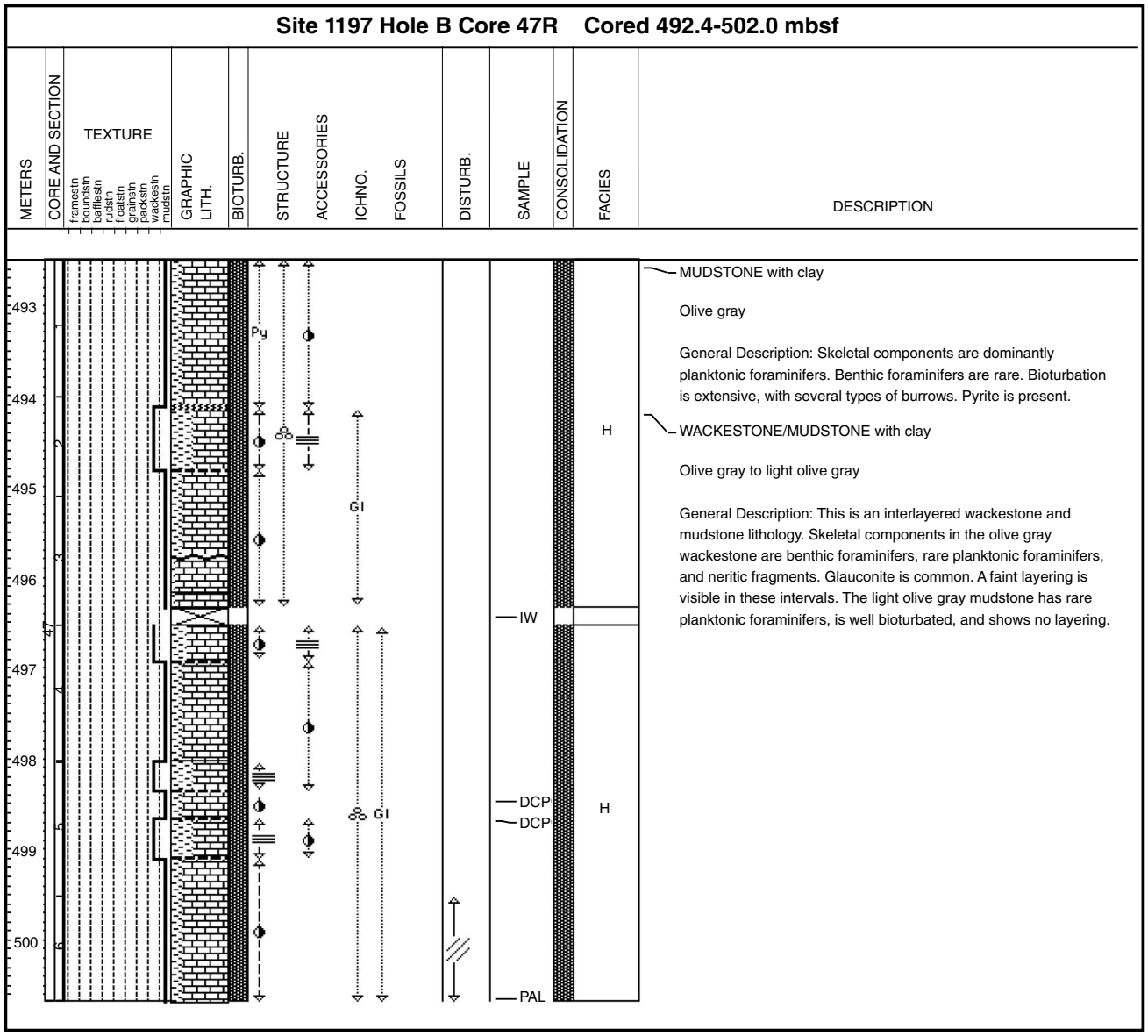

Figure F7. Graphic symbols used by Leg 194 sedimentologists in the barrel sheets.

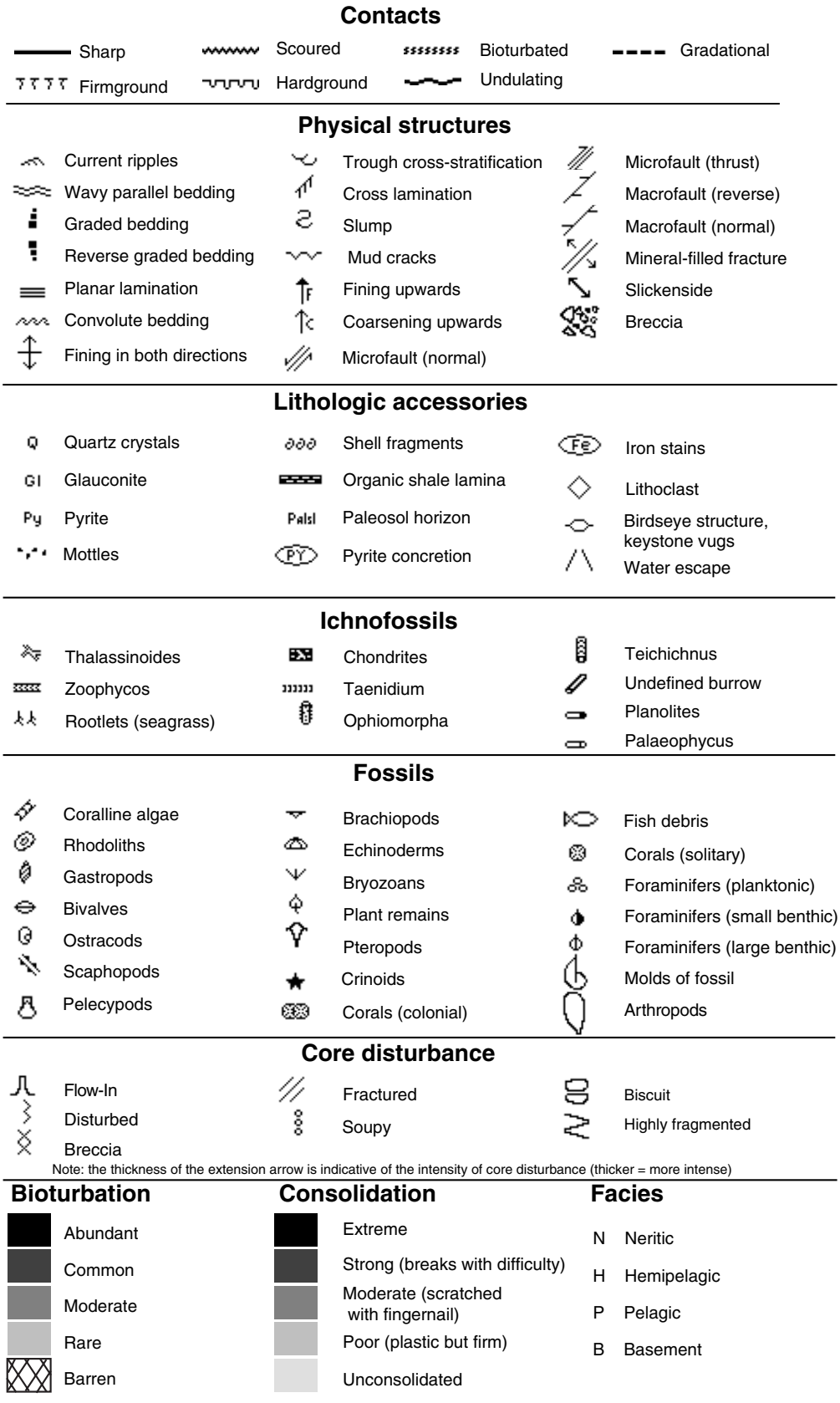

Figure F8. Planktonic foraminifer ages employed during Leg 194. FO = first occurence, LO = last occurrence.

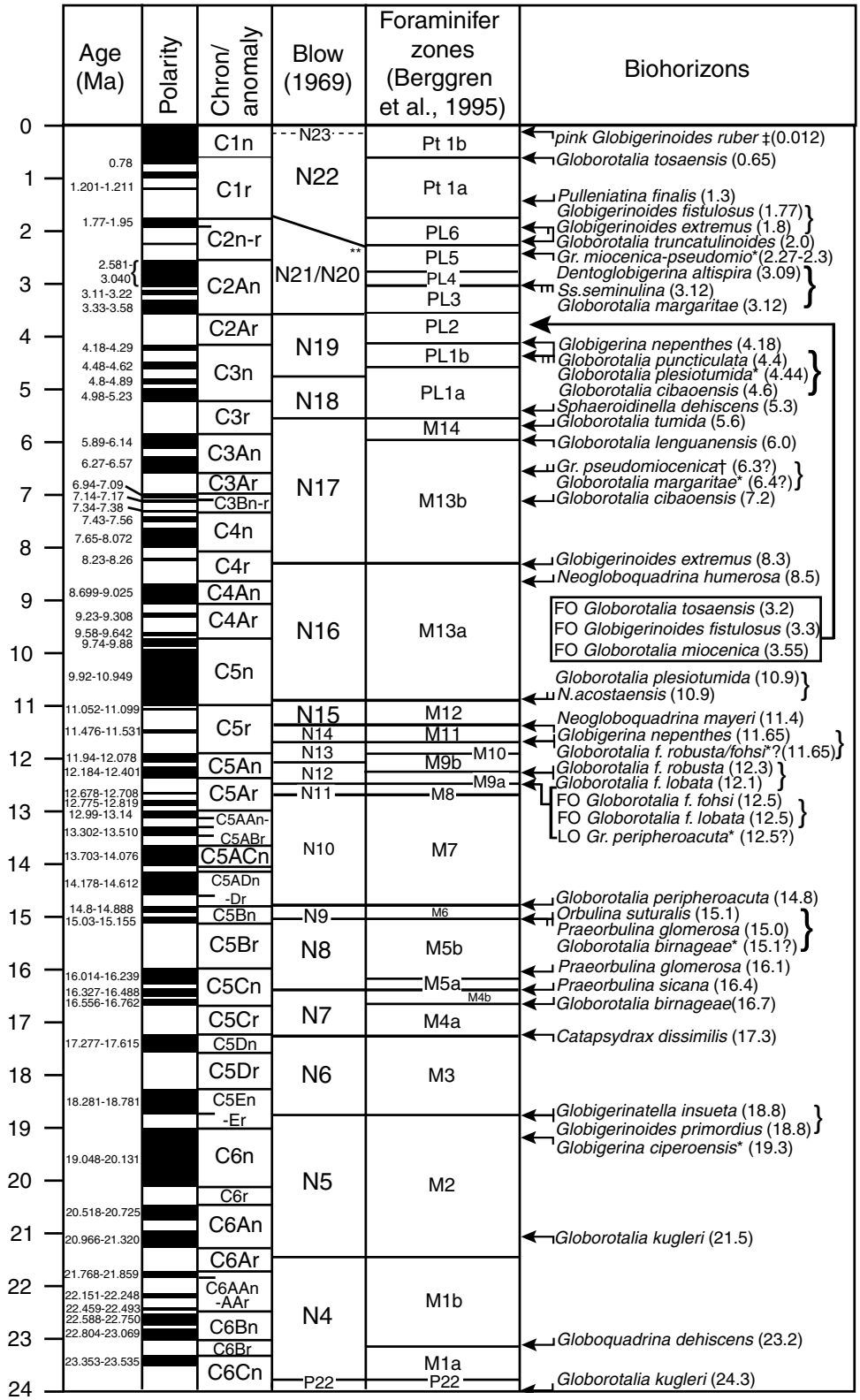

† - Datum from Bolli & Saunders, 1980.
‡ - Datum from Berggren, Kent & Van Couvering, 1985b.
* - Datum from Kennett & Srinivasan, 1983.
** - Isochronous boundary from Spencer-Cervato, 1997 and Chaisson, 1997.

Figure F9. Magnetic orientation convention.

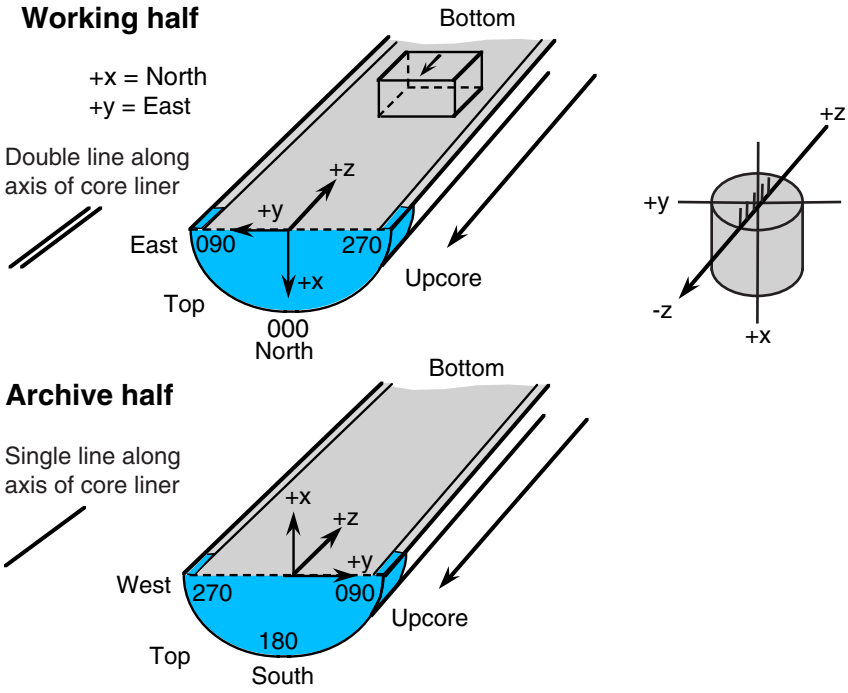

Figure F10. Schematic illustration of the configurations of tool strings run during Leg 194. MGT = multisensor natural gamma ray tool, HNGS = spectral gamma ray, APS = accelerator porosity sonde, HLDT = hostile lithodensity logging tool, DITE = digital dual induction tool, TAP = temperature, acceleration, pressure tool, NGT = natural gamma spectrometry tool, LSS = long-spaced sonic logging tool, GPIT = general purpose inclinometer tool, FMS = Formation MicroScanner.

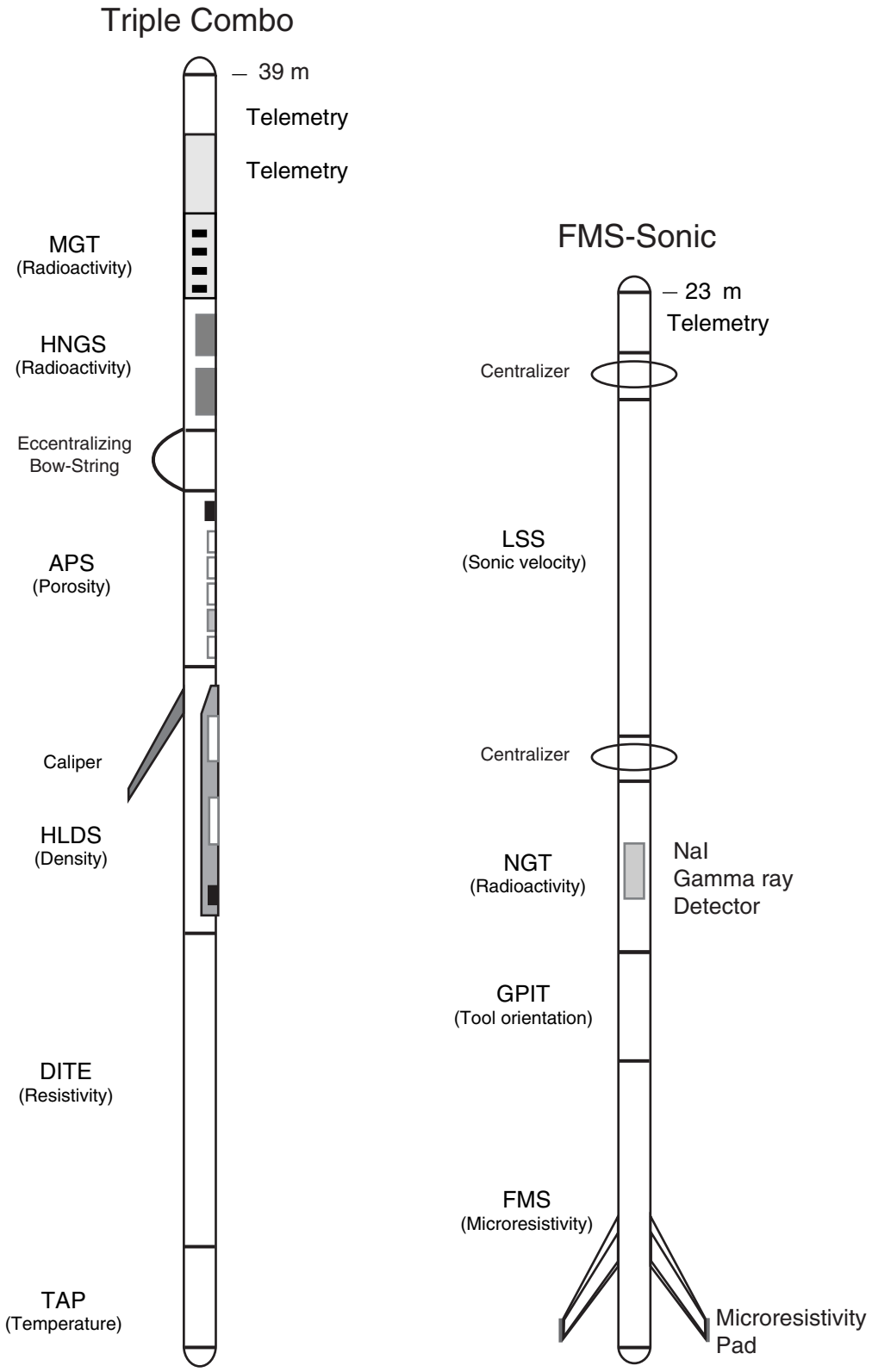

Figure F11. LDEO multisensor gamma ray tool.

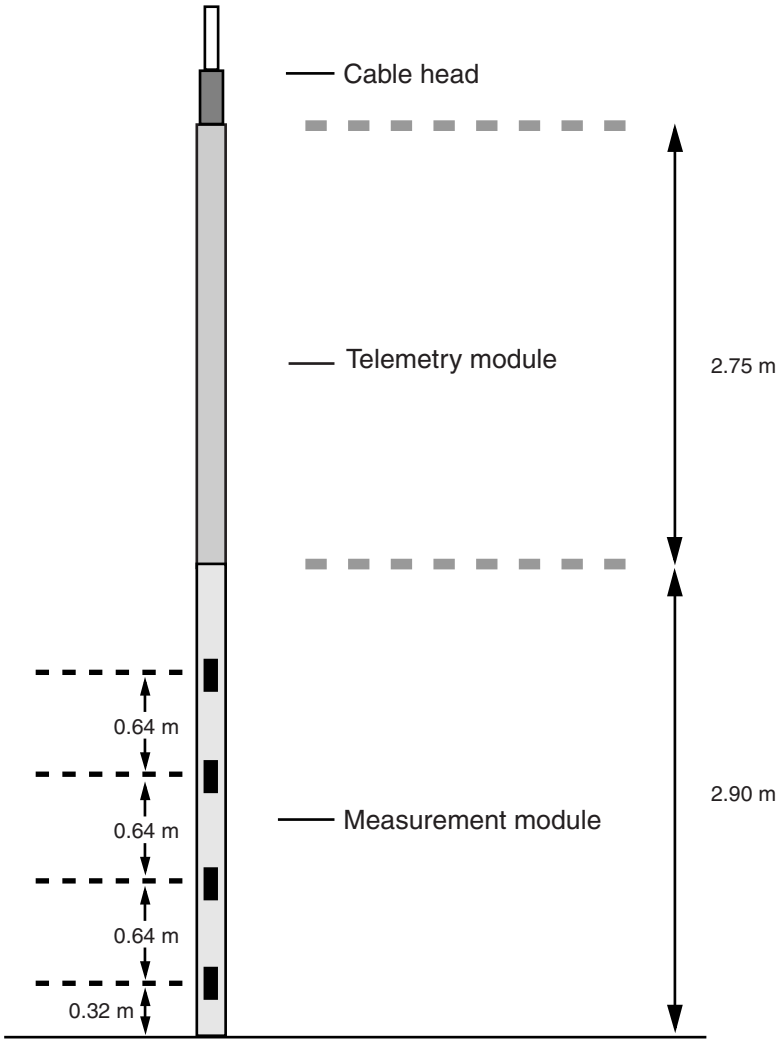

Table T1. Comparison of core barrels.

Parameter	RCB	DCB	ADCB
Hole diameter (in)	9.88	7.25	7.25
Core diameter (in)	2.31	2.31	3.27 or 3.35
Hole cross section (in^2)	75.20	41.28	41.28
Core cross section (in^2)	4.20	4.20	8.40 or 8.79
Area of material removed (in^2)	72.39	37.08	32.49 or 32.88
Kerf (outer diameter minus inner diameter) (in)	3.78		1.95

Note: RCB = rotary core barrel, DCB = diamond core barrel, ADCB = advanced diamond core barrel.

Table T2. Checklist to assist in the completion of visual core description forms.

1. Double check site/core/hole
2. Describe sediment/rock type:
   a. Estimate proportion of carbonate vs. siliciclastic sediment (e.g., 20% clay and 80% carbonate)
   b. Identify main constituents (e.g., skeletal, nonskeletal, quartz)
   c. Assign principal name (e.g., skeletal grainstone, grainstone with clay)
   d. Add size modifier if necessary (e.g., silt-sized)
   e. Estimate dolomite content
3. Describe color
4. Describe bioturbation
5. Describe fossils and ichnofossils
6. Describe the consolidation:
   Extreme = impossible to scratch or break
   Strong = scratches or breaks with difficulty
   Moderate = scratches or breaks easily
   Poor = firm, resistance to finger pressure, reduced water content
   Unlithified = soft with little strength, easily deformed, high water content
7. Describe sedimentary structures
8. Describe sorting
9. Qualitative description of porosity
10. Describe core disturbance
11. Provide a record of all samples taken (e.g., photos, thin sections, smear slides)
12. Assign minor modifiers (e.g., bioclast type)
13. Describe facies and downcore changes in facies (e.g., Pelagic, Hemipelagic, Neritic)
14. Circle your initials
15. Repeat procedure with the next core

Table T3. Biostratigraphic ranges of selected larger foraminifers in northern Australia.

Planktonic foraminiferal zone:	N3/N4	N3/N4	N5	N6	N6	N7/N8	N9	N9	N10	N11	N12	late	
Larger foraminiferal association:	LF1	LF2	LF3	LF4	LF5	LF6	LF7	LF8				Miocene	Holocene
Taxon:													
Austrotrillina howchini							X	X					
Austrotrillina striata		X											
Lacazinella sp. cf. L. *wichmanni*	X												
Flosculinella bontangensis								X					
Operculina complanata	X	X	X	X	X	X	X	X	X	X	X	X	X
Operculinella venosa						X	X	X					
Cycloclypeus spp.		X	X	X	X	X	X	X	X	X	X	X	X
Cycloclypeus annulatus						X	X						
Heterostegina borneensis	X	X											
Heterostegina suborbicularis						X							
Spiroclypeus sp. cf. *S. margaritatus*		X											
Miogypsina globulina		X											
Miogypsina intermedia		X											
Miogypsina thecideaeformis			X	X	X	X	X	X					
Miogypsina dehaarti		X	X	X	X	X							
Amphistegina bikiniensis	X	X											
Amphistegina hauerina					X	X	X	X					
Amphistegina spp.	X	X	X	X	X	X	X	X	X	X	X	X	X
Gypsina globulus		X		X	X	X	X	X					
Gypsina howchini	X	X				X	X	X					
Gypsina mastaelensis							X	X					
Gypsina sp.					X	X							
Lepidocyclina badjirraensis					X								
Lepidocyclina ephippoides	X	X											
Lepidocyclina howchini	X	X	X	X	X	X	X	X	X	X	X	X	
Lepidocyclina japonica					X								
Lepidocyclina orakeiensis waikukuensis						X							
Lepidocyclina orakeiensis orakeiensis		X											
Lepidocyclina sumatrensis		X											

Note: Adapted from Chaproniere (1981, 1984) and modified after Chaproniere and Betzler (1993) and Betzler (1997).

Table T4. Benthic foraminifers noted for paleoenvironmental analysis.

Outer neritic/bathyal taxa	Inner-middle neritic taxa	Milioline euphotic taxa	Rotaliine euphotic taxa
Anomalinoides spp.	*Ammonia* spp.	*Marginopora* spp.	*Amphistegina* spp.
Cibicidoides spp.	*Discorbis* spp.	*Sorites* spp.	*Cycloclypeus* spp.
Hoeglandina elegans	*Elphidium* spp.	*Cyclorbiculina* (?) sp.	*Gypsina* spp.
Laticarinina pauperata	*Miliolinella* spp.	*Peneroplis* spp.	*Heterostegina* spp.
Lenticulina spp.	*Planorbulina* spp.	*Flosculinella botangensis*	*Lepidocyclina* spp.
Planulina spp.	*Quinqueloculina* spp.	*Borelis* spp.	*Miogypsina* spp.
Rectuvigerina spp.	*Triloculina* spp.	Other	*Operculina complanata*
Sigmoilopsis schlumbergeri	Other		Other
Siphonina sp.			
Uvigerina spp.			
Nodosaridae			
Tubular agglutinated taxa			
Other			

Table T5. Constituents and characteristics noted for paleoenvironmental analysis.

Pelagic taxa	Benthic foraminifers*	Macrofauna	Algae	Coral	Carbonate debris	Non-carbonates	Preservation
Planktonic foraminfers Pteropods	Outer neritic/upper bathyal taxa Inner-middle neritic smaller taxa Miloline larger foraminifers Rotaliine larger foraminifers	Bryozoans Bivalves Gastropods Echinoids Other	Rhodoliths Red algal fragments *Halimeda* Other	Solitary Colonial	Planktonic Neritic Nondescript	Quartz Rock fragments Glauconite Phosphatic grains Other	Broken Rounded Altered Recrystallized Glauconite-filled Phosphatized Blackened Other

Note: * = see Table **T4,** p. 54.

Table T6. Thermal conductivity of water and sediment types (Beaumont and Keen, 1990).

Material	Water	Shale	Limestone	Sandstone
Thermal conductivity (W/[m·K])	0.61	1.13	2.929	4.184

Table T7. Specifications of the logging tools deployed, Leg 194.

Tool string	Typical logging speed (m/hr)	Tool	Measurement	Sample interval (cm)	Approximate vertical resolution (cm)
Run 1: Triple combination	250–275	MGT	Multisensor natural gamma ray	1.5	~10
(total length ~36.05 m)		HNGS*	Natural gamma ray	15	45
		APS*	Porosity	5 and 15	30
		HLDS*	Bulk density, PEF	15	38
		DITE*	Resistivity	15	61
		TAP	Temperature,	1/s	NA
			acceleration,	4/s	NA
			pressure	1/s	NA
Run 2: FMS-sonic	250–275				
(total length ~33.4 m)		NGT*	Natural gamma ray	15	45
		GPIT*	Magnetic orientation	0.25	NA
		LSS*	Sonic velocity	15	120
		FMS*	Resistivity image	0.25	0.5
Run 3: WST	Stationary	WST*	Sonic traveltime	3000–5000	NA

Notes: * = trademarks of Schlumberger. See Table **T8,** p. 58, for explanations of the acronyms. PEF = photoelectric effect factor, NA = not assigned.

Table T8. Logging tools and log acronyms, Leg 194.

Tool	Output	Explanation	Units
HNGS*		Hostile-environment spectral gamma ray sonde	
	HSGR	Standard (total) gamma ray	gAPI
	HCGR	Computed gamma ray (HSGR – uranium contribution)	gAPI
	HFK	Formation potassium	wt%
	HTHO	Thorium	ppm
	HURA	Uranium	ppm
NGT*		Natural gamma ray tool	
	SGR	Standard total gamma ray	gAPI
	CGR	Computed gamma ray (SGR – uranium contribution)	gAPI
	POTA	Potassium	wt%
	THOR	Thorium	ppm
	URAN	Uranium	ppm
MGT		Multisensor natural gamma ray tool	
	SGR	Standard total gamma ray	gAPI
	CGR	Computed gamma ray (SGR – uranium contribution)	gAPI
	POTA	Potassium	wt%
	THOR	Thorium	ppm
	URAN	Uranium	ppm
APS		Accelerator porosity sonde	
	APLC	Near array porosity (limestone corrected)	pu
	FPLC	Far array porosity (limestone corrected)	pu
	SIGF	Neutron capture cross section of the formation (Sf)	cu
	STOF	Tool standoff (computed distance from borehole wall)	in
HLDS		High-temperature lithodensity sonde	
	RHOM	Bulk density (corrected)	g/cm^3
	PEFL	Photoelectric effect factor	$barn/e^-$
	LCAL	Caliper-measure of borehole diameter	in
	DRH	Bulk density correction	g/cm^3
DITE		Dual induction tool	
	ILD	Deep resistivity	Ωm
	ILM	Medium resistivity	Ωm
	SFLU	Shallow resistivity	Ωm
TAP		High-resolution temperature/acceleration/pressure tool	
	TAP	Temperature/acceleration/pressure	°C, mm/s^2, psi
LSS		Long-spaced sonic tool	
	V_P	Compressional wave velocity	µs/ft
FMS*		Formation MicroScanner Resistivity image	
GPIT*		General purpose inclinometer tool	
	Hazi	Hole azimuth	Degree
	FNOR	Intensity of the total magnetic field	oer
WST		Well seismic tool	
	Dt	Acoustic arrival times	µs

Note: * = trademark of Schlumberger.